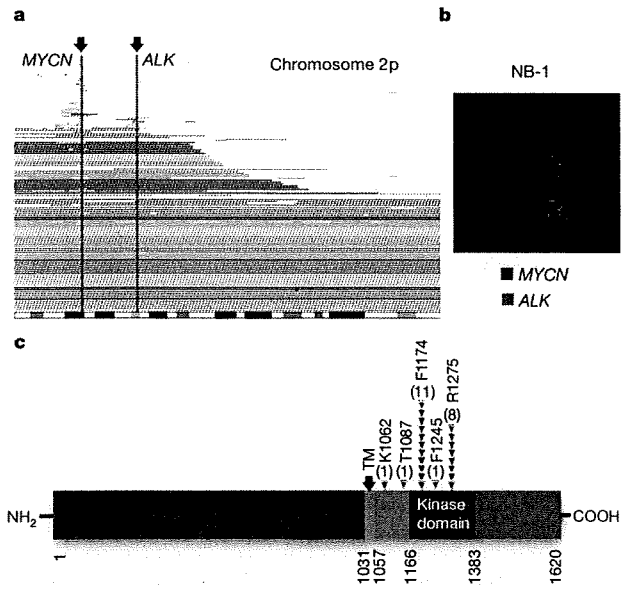

Figure 1 | Common 2p gains/amplifications and *ALK* mutations in neuroblastoma samples. **a**, Recurrent copy number gains on the 2p arm. High-grade amplifications are shown by light-red horizontal lines, whereas simple gains are shown by dark-red lines. Two common peaks of copy number gains and amplifications in the *MYCN* and *ALK* loci are indicated by arrows. The cytobands in 2p are shown at the bottom. **b**, Interphase FISH analysis of NB-1 showing high-grade amplification of *MYCN* (red) and *ALK* loci (green). The amplified *MYCN* locus appears as a single large signal. **c**, Distribution of the eight *ALK* mutations found in 21 neuroblastoma samples. The positions of the mutated amino acids are indicated by black (primary samples) and red (cell lines) arrowheads. The number of mutations at each site is shown at the top of the arrowheads. TM, transmembrane.

(6.1%) primary samples and 8 out of 24 (33%) cell lines, which resulted in seven types of amino acid substitutions at five different positions (Table 1 and Supplementary Fig. 6). They were not found in either the genomic DNA collected from 50 healthy volunteers or in the SNP databases at the time of preparing this manuscript. In fact, somatic origins of missense changes were confirmed in 9 out of 13 primary cases, for which DNA was obtained from the peripheral blood or the tumour-free bone marrow specimens (Supplementary Fig. 6). On the other hand, T1087I (ACC>ATC), found in case NT126, had a germline origin and thus it could not be determined whether the T1087I change was a rare non-functional polymorphism or represented a pathogenic germline mutation. For other changes found in three primary cases (NT128, NT217 and NT218) and cell lines, normal DNA was not available but they were likely to represent oncogenic mutations because they were identical to common somatic changes (F1174L or R1275Q) or shown to have oncogenic potential in functional assays (K1062M).

Most mutations occurred within the kinase domain (20 out of 22 or 91%), which clearly showed two mutation hotspots at F1174 and R1275 (Fig. 1c). A neuroblastoma-derived cell line, SJNB-2, had a homozygous *ALK* mutation of R1275Q, which was probably due to uniparental disomy of chromosome 2 (Supplementary Fig. 7a). Another case (NT074) harboured two different mutations, F1174L and R1275Q, but it remains to be determined whether both are on the same allele. ALK mutations within the kinase domain occurred at amino acid positions that are highly conserved across species and during molecular evolution (Supplementary Figs 8 and 9). According to the conserved structure of other insulin receptor kinases we predicted that F1174 is located at the end of the Cα1 helix, whereas the other two are on the two β-sheets: before the catalytic loop (β6, F1245) and within the activation loop (β9, R1275) (Supplementary Fig. 7b, c)[17]. Thus, conformational changes due to amino acid substitutions at these positions might be responsible for the aberrant activity of the mutant kinases.

Table 1 | *ALK* mutations/amplifications in neuroblastoma samples

Sample	Age (months)	Stage	*MYCN**	Clinical outcome	Mutations/ amplifications	Nucleotide substitution	Origin of mutations
NT126	99	4	−	Dead	T1087I	ACC>ATC	Germ line
NT218	8	1	−	Alive	F1174L	TTC>TTG	ND
NT074	34	3	+	Dead	F1174L	TTC>TTA	Somatic
					R1275Q	CGA>CAA	
NT160	12	4	+	Dead	F1174L	TTC>TTA	Somatic
NT217	24	4	+	Dead	F1174L	TTC>TTA	ND
NT190	48	4	+	Alive	F1174L	TTC>TTA	Somatic
NT060	163	3	−	Alive	F1174C	TTC>TGC	Somatic
NT162	28	4	+	Dead	F1174V	TTC>GTC	Somatic
NT195	24	4	+	Alive	F1245L	TTC>TTG	Somatic
NT055	6	3	−	Alive	R1275Q	CGA>CAA	Somatic
NT128	8	4	−	Dead	R1275Q	CGA>CAA	ND
NT164	54	4	+	Dead	R1275Q	CGA>CAA	Somatic
NT200	133	4	−	Dead	R1275Q	CGA>CAA	Somatic
SCMC-N5†	-	-	+	-	K1062M	AAG>ATG	ND
SJNB-4†	-	-	+	-	F1174L	TTC>TTA	ND
LAN-1†	-	-	+	-	F1174L	TTC>TTA	ND
SCMC-N2†	-	-	+	-	F1174L	TTC>TTA	ND
SK-N-SH†	-	-	−	-	F1174L	TTC>TTA	ND
SJNB-2†‡	-	-	+	-	R1275Q	CGA>CAA	ND
LAN-5†	-	-	+	-	R1275Q	CGA>CAA	ND
TGW†	-	-	+	-	R1275Q	CGA>CAA	ND
NT204	12	1	+	Alive	Amplification	-	-
NT056	11	3	−	Dead	Amplification	-	-
NT071	36	3	+	Alive	Amplification	-	-
NT165	19	4	+	Dead	Amplification	-	-
NT169	7	4	+	Dead	Amplification	-	-
NB-1†	-	-	+	-	Amplification	-	-

ND, not determined.
* Presence (+) or absence (−) of *MYCN* amplification in FISH analysis. All cases where there was an absence of *MYCN* amplification (−) were also checked for possible *MYCN* mutations by sequencing of all *MYCN* exons, but no *MYCN* mutations were identified.
† Cell lines.
‡ Homozygous mutation.

ALK mutation highly correlated with *MYCN* amplification ($P = 1.55 \times 10^{-4}$, Fisher's exact test; Supplementary Table 6) where 14 out of 21 mutations coexisted with *MYCN* amplification. Regardless of the status of *MYCN* amplification, 12 of the 13 mutations were found in patients with advanced stage neuroblastoma (Table 1). However, whereas *MYCN* amplification and stage 4 were significant risk factors for poor survival, the mutation/amplification status of *ALK* was not likely to have a major impact on survival (Supplementary Fig. 10 and Supplementary Table 7), although the statistical power of the current analysis was largely limited in order to detect a marginal hazard.

To evaluate the impact of ALK mutations on kinase activity, we generated Flag-tagged constructs of ALK and its mutants, F1174L and K1062M, which were stably expressed in NIH3T3 cells, and examined their phosphorylation status and *in vitro* kinase activity. The ALK mutants stably expressed in NIH3T3 cells were phosphorylated according to western blot analysis using an antibody specific for phosphorylated ALK (anti-pY1604) and a PY20 blot after anti-Flag immunoprecipitation of the mutant kinases (Fig. 2a), whereas the wild-type kinase was not phosphorylated. The immunoprecipitated ALK mutants also showed increased tyrosine kinase activity *in vitro* when compared with wild-type ALK. This was shown using both a universal substrate for tyrosine kinase (poly-GluTyr) and the synthetic YFF peptide[18], which was derived from a sequence of the activation loop of *ALK* (Fig. 2b, c). In accordance with these findings, downstream molecules of ALK signalling including AKT, STAT3 and ERK[15] were activated in cells expressing mutant ALK, as shown by their increased phosphorylation (Fig. 2d).

Next, we investigated the oncogenic potential of these mutants. NIH3T3 cells stably expressing mutant kinases showed increased colony formation in soft agar compared with the wild-type protein (Fig. 3a and Supplementary Fig. 11). The tumorigenicity of these ALK mutants was further assayed by injecting 1.0×10^7 NIH3T3 cells into nude mice. The NIH3T3 cells transfected with the ALK mutants showed focus-forming capacity and developed subcutaneous tumours (6 out of 6 inoculations) 21 days after inoculation, whereas the mock and wild-type ALK-transfected cells did not (0 out of 6 inoculations) (Fig. 3b, c). Finally, we examined the effect of ALK inhibition on the proliferation of neuroblastoma-derived cell lines. RNA interference (RNAi)-mediated *ALK* knockdown resulted in reduced cell proliferation of SK-N-SH cells harbouring the F1174L mutation, but the effects were less clear in wild-type ALK-expressing LAN-2 cells (Fig. 3d, e). Of particular interest is a recent report that 5 out of 17 neuroblastoma-derived cell lines, including SK-N-SH and NB-1, frequently showed high sensitivity to the specific ALK inhibitor TAE684 (ref. 19).

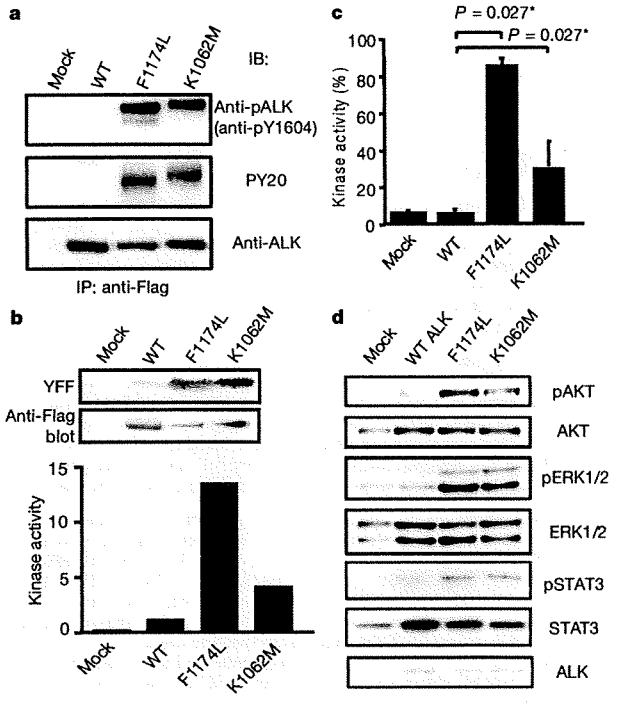

Figure 2 | Kinase activity of ALK mutants and their downstream signalling. **a**, Stably expressed ALK and its mutants (F1174L and K1062M) were immunoprecipitated with an anti-Flag antibody and subjected to western blot analysis with anti-pY1604 (upper panel) or PY20 (middle panel). An anti-ALK blot of precipitated kinases is also displayed (bottom panel). **b**, *In vitro* kinase assay for wild-type ALK kinase and its mutants using the synthetic YFF peptide as a substrate, where kinase activity is expressed as relative values to that for wild-type kinase based on the densities in the autoradiogram. **c**, Kinase activity was also assayed for the poly-GluTyr peptide. Significantly different measurements are indicated by asterisks with *P* values. Bars show mean (±s.d.) in three independent experiments. **d**, Western blot analyses of NIH3T3 cells expressing wild-type and mutant ALK for phosphorylated forms of AKT (pAKT), ERK (pERK1/2) and STAT3 (pSTAT3). The total amount of each molecule is also displayed (AKT, ERK1/2, and STAT3) together with an anti-ALK blot (ALK).

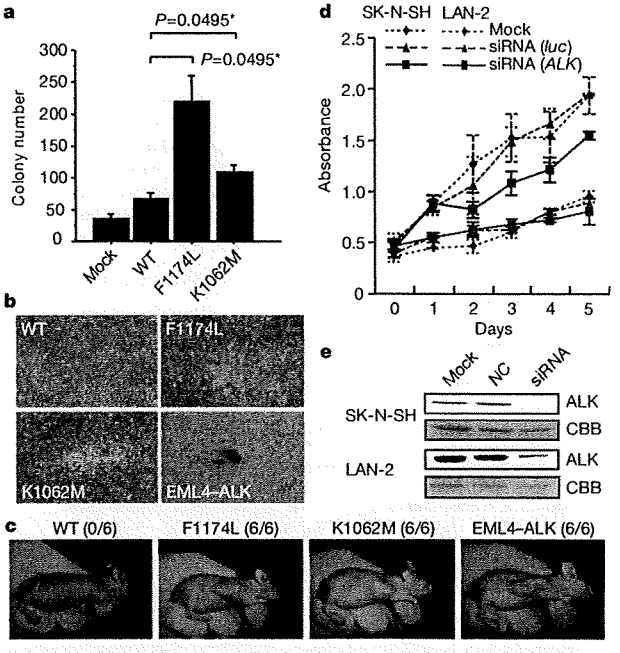

Figure 3 | Oncogenic role of ALK mutations. **a**, Colony assays for NIH3T3 cells stably expressing wild-type as well as mutant ALK (F1174L and K1062M). The average numbers of colonies in triplicate experiments are plotted and standard deviation is indicated. Results showing statistically significant differences as compared with experiments using wild-type ALK are indicated by asterisks with *P* values. **b**, **c**, NIH3T3 cells were transfected with wild-type and mutant ALK (F1174L, K1062M and EML4–ALK) and subjected to a focus forming assay (**b**) as well as an *in vivo* tumorigenicity assay in nude mice (**c**). **d**, Effect of RNAi-mediated ALK knockdown on cell proliferation in neuroblastoma cell lines expressing either the F1174L mutant (SK-N-SH) or wild-type ALK (LAN-2). Cell growth was measured using the Cell Counting Kit-8 after knockdown experiments using *ALK*-specific siRNAs (siRNA *ALK*), control siRNAs (siRNA *luc*), or mock experiments, where absorbance was measured in triplicate and averaged for each assay. To draw growth curves, the mean ± s.d. of the averaged absorbance in three independent knockdown experiments is plotted. **e**, Successful knockdown of ALK protein was confirmed by anti-ALK blots (ALK) using Coomassie brilliant blue G-250 (CBB) staining as loading controls. NC, control siRNA; siRNA, *ALK* siRNA.

Through the genome-wide analysis of genetic lesions in neuroblastoma, we identified novel oncogenic *ALK* mutations in advanced neuroblastoma. Combined with the cases having a high-grade amplification of the *ALK* gene, aberrant ALK signalling was likely to be involved in 11% (16 out of 151) of the advanced neuroblastoma cases. Because ALK kinase has been shown to be deregulated only in the form of a fusion kinase in human cancers, including lymphoma and lung cancer, the identification of oncogenic mutations in *ALK* not only increases our understanding of the molecular pathogenesis of advanced neuroblastoma, but also adds a new paradigm to the concept of 'ALK-positive human cancers' in that the mutated *ALK* kinases themselves might participate in human cancers. Our results again highlight the power of genome-wide studies to clarify the genetic lesions in human cancers[20–22]. Given that *ALK* mutations are preferentially involved in advanced neuroblastoma cases having a poor prognosis, our findings implicate that *ALK* inhibitors may improve the clinical outcome of children suffering from intractable neuroblastoma.

METHODS SUMMARY

Genomic DNA from 215 patients with primary neuroblastoma and 24 neuroblastoma-derived cell lines was analysed on GeneChip SNP genotyping microarrays (Affymetrix GeneChip 250K *Nsp*I). After appropriate normalization of mean array intensities, signal ratios were calculated between tumours and anonymous normal references in an allele-specific manner, and allele-specific copy numbers were inferred from the observed signal ratios based on the hidden Markov model using CNAG/AsCNAR software[13,14]. *ALK* mutations were examined by DNA heteroduplex analysis and/or genomic DNA sequencing[16]. Full-length cDNAs for mutant *ALK* were isolated by high-fidelity PCR and inserted into pcDNA3 and pMXS. The expression plasmids were transfected into NIH3T3 cells using Effectene Transfection Reagent (Qiagen) or by calcium phosphate methods[9]. Western blot analysis of mutant ALK kinases, *in vitro* kinase assays, and tumour formation assays in nude mice were performed as previously described[9]. This study was approved by the ethics boards of the University of Tokyo and of the Chiba Cancer Center Research Institute.

Full Methods and any associated references are available in the online version of the paper at www.nature.com/nature.

Received 3 June; accepted 28 August 2008.

1. Maris, J. M., Hogarty, M. D., Bagatell, R. & Cohn, S. L. Neuroblastoma. *Lancet* 369, 2106–2120 (2007).
2. Maris, J. M. *et al.* Loss of heterozygosity at 1p36 independently predicts for disease progression but not decreased overall survival probability in neuroblastoma patients: a Children's Cancer Group study. *J. Clin. Oncol.* 18, 1888–1899 (2000).
3. Attiyeh, E. F. *et al.* Chromosome 1p and 11q deletions and outcome in neuroblastoma. *N. Engl. J. Med.* 353, 2243–2253 (2005).
4. Bown, N. *et al.* Gain of chromosome arm 17q and adverse outcome in patients with neuroblastoma. *N. Engl. J. Med.* 340, 1954–1961 (1999).
5. Brodeur, G. M., Seeger, R. C., Schwab, M., Varmus, H. E. & Bishop, J. M. Amplification of N-myc in untreated human neuroblastomas correlates with advanced disease stage. *Science* 224, 1121–1124 (1984).
6. Shiota, M. *et al.* Anaplastic large cell lymphomas expressing the novel chimeric protein p80NPM/ALK: a distinct clinicopathologic entity. *Blood* 86, 1954–1960 (1995).
7. Morris, S. W. *et al.* Fusion of a kinase gene, ALK, to a nucleolar protein gene, NPM, in non-Hodgkin's lymphoma. *Science* 263, 1281–1284 (1994).
8. Fujimoto, J. *et al.* Characterization of the transforming activity of p80, a hyperphosphorylated protein in a Ki-1 lymphoma cell line with chromosomal translocation t(2;5). *Proc. Natl Acad. Sci. USA* 93, 4181–4186 (1996).
9. Soda, M. *et al.* Identification of the transforming *EML4–ALK* fusion gene in non-small-cell lung cancer. *Nature* 448, 561–566 (2007).
10. Rikova, K. *et al.* Global survey of phosphotyrosine signaling identifies oncogenic kinases in lung cancer. *Cell* 131, 1190–1203 (2007).
11. Kennedy, G. C. *et al.* Large-scale genotyping of complex DNA. *Nature Biotechnol.* 21, 1233–1237 (2003).
12. Matsuzaki, H. *et al.* Genotyping over 100,000 SNPs on a pair of oligonucleotide arrays. *Nature Methods* 1, 109–111 (2004).
13. Nannya, Y. *et al.* A robust algorithm for copy number detection using high-density oligonucleotide single nucleotide polymorphism genotyping arrays. *Cancer Res.* 65, 6071–6079 (2005).
14. Yamamoto, G. *et al.* Highly sensitive method for genomewide detection of allelic composition in nonpaired, primary tumor specimens by use of affymetrix single-nucleotide-polymorphism genotyping microarrays. *Am. J. Hum. Genet.* 81, 114–126 (2007).
15. Osajima-Hakomori, Y. *et al.* Biological role of anaplastic lymphoma kinase in neuroblastoma. *Am. J. Pathol.* 167, 213–222 (2005).
16. Donohoe, E. Denaturing high-performance liquid chromatography using the WAVE DNA fragment analysis system. *Methods Mol. Med.* 108, 173–187 (2005).
17. Hu, J., Liu, J., Ghirlando, R., Saltiel, A. R. & Hubbard, S. R. Structural basis for recruitment of the adaptor protein APS to the activated insulin receptor. *Mol. Cell* 12, 1379–1389 (2003).
18. Donella-Deana, A. *et al.* Unique substrate specificity of anaplastic lymphoma kinase (ALK): development of phosphoacceptor peptides for the assay of ALK activity. *Biochemistry* 44, 8533–8542 (2005).
19. McDermott, U. *et al.* Genomic alterations of anaplastic lymphoma kinase may sensitize tumors to anaplastic lymphoma kinase inhibitors. *Cancer Res.* 68, 3389–3395 (2008).
20. Garraway, L. A. *et al.* Integrative genomic analyses identify MITF as a lineage survival oncogene amplified in malignant melanoma. *Nature* 436, 117–122 (2005).
21. Mullighan, C. G. *et al.* Genome-wide analysis of genetic alterations in acute lymphoblastic leukaemia. *Nature* 446, 758–764 (2007).
22. Kawamata, N. *et al.* Molecular allelokaryotyping of pediatric acute lymphoblastic leukemias by high-resolution single nucleotide polymorphism oligonucleotide genomic microarray. *Blood* 111, 776–784 (2008).

Supplementary Information is linked to the online version of the paper at www.nature.com/nature.

Acknowledgements We thank H. P. Koeffler for critically reading and editing the manuscript. We also thank M. Matsumura, Y. Ogino, S. Ichimura, S. Sohma, E. Matsui, Y. Yin, N. Hoshino and Y. Nakamura for their technical assistance. This work was supported by the Core Research for Evolutional Science and Technology, Japan Science and Technology Agency and by a Grant-in-Aid from the Ministry of Health, Labor and Welfare of Japan for the third-term Comprehensive 10-year Strategy for Cancer Control.

Author Contributions Y.C., Y.L.C. and J.T. contributed equally to this work. M.K. and M.Sa. performed microarray experiments and subsequent data analyses. Y.C. and J.T. performed mutation analysis of *ALK*. Y.C., Y.L.C., J.T., M.So., L.W. and H.M. conducted functional assays of mutant ALK. A.N., M.O., T.I., A.K. and Y.H. prepared tumour specimens and were involved in statistical analysis. A.N., Y.H., H.M., J.T. and S.O. designed the overall study, and S.O. and J.T. wrote the manuscript. All authors discussed the results and commented on the manuscript.

Author Information The nucleotide sequences of *ALK* mutations detected in this study have been deposited in GenBank under the accession numbers EU788003 (K1062M), EU788004 (T1087I), EU788005 (F1174L; TTC/TTA), EU788006 (F1174L; TTC/TTG), EU788007 (F1174C), EU788008 (F1174V), EU788009 (F1245L) and EU788010 (R1275Q). The copy number data as well as the raw microarray data will be accessible from http://www.ncbi.nlm.nih.gov/geo/ with the accession number GSE12494. Reprints and permissions information is available at www.nature.com/reprints. Correspondence and requests for materials should be addressed to S.O. (sogawa-tky@umin.net) or Y.H. (hayashiy-tky@umin.ac.jp).

METHODS

Specimens. Primary neuroblastoma specimens were obtained during surgery or biopsy from patients who were diagnosed with neuroblastoma and admitted to a number of hospitals in Japan. In total, 215 primary neuroblastoma specimens were subjected to SNP array analysis after informed consent was obtained from the parents of each patient. The patients were staged according to the International Neuroblastoma Staging System[23]. The clinicopathological findings are summarized in Supplementary Table 1. Twenty-four neuroblastoma-derived cell lines were also analysed by SNP array analysis (Supplementary Table 2). The SCMC-N2, SCMC-N4 and SCMC-N5 cell lines were established in our laboratory[24,25]. The SJNB series of cells and the UTP-N-1[26] cell line were gifts from A. T. Look and A. Inoue, respectively. The other cell lines used were obtained from the Japanese Cancer Resource Cell Bank (http://cellbank.nibio.go.jp/).

Microarray analysis. High molecular mass DNA was isolated from tumour specimens as well as from the peripheral blood or the bone marrow as described previously[24]. The DNA was subjected to SNP array analysis using Affymetrix GeneChip Mapping 50K and/or 250K arrays (Affymetrix) according to the manufacturer's suggested protocol. The scanned array images were processed with Gene Chip Operation software (GCOS)[13], followed by SNP calls using GTYE. Genome-wide copy number measurements and loss of heterozygosity detection were performed using CNAG/AsCNAR algorithms[14], which enabled an accurate determination of allele-specific copy numbers.

Confirmation of SNP array data. FISH and/or genomic PCR analysis confirmed the results of SNP array analyses as described previously[13]. PCR primer sets were designed to amplify several adjacent fragments inside and outside of the homozygously deleted regions in tumour samples.

Mutation analysis. Mutations in the *ALK* gene were examined in 239 neuroblastoma samples, including 24 cell lines, by denaturing high-performance liquid chromatography (DHPLC) using the WAVE system (Model 4500; Transgenomic) according to the manufacturer's suggested protocol[16]. The samples showing abnormal conformations were subjected to direct sequencing analysis using an ABI PRISM 3100 Genetic Analyser (Applied Biosystems). Using direct sequencing, mutation analysis of *MYCN* was also performed in seven cases with *ALK* alterations but not *MYCN* amplification. The primer sets used in this study are listed in Supplementary Table 5.

Transforming potential of *ALK* mutants. Total RNA was extracted from SJNB-1 (wild type), SCMC-N2 (F1174L) and SCMC-N5 (K1062M) cells as described previously[26]. First-strand cDNA was synthesized from RNA using Transcriptor Reverse Transcriptase and an oligo (dT) primer (Roche Applied Science). The resulting cDNA was then amplified by PCR using the KOD-Plus-Ver.2 DNA polymerase (Toyobo) and the primers sense 5′-TCAGAAGCTTTACCAAGGACTGTTCAGAGC-3′ and antisense 5′-AATTGCGGCCGCTACTTGTCATCGTCGTCCTTGTAGTCGGGCCCAGGCTG GTTCATGC-3′, thereby introducing a HindIII site at the 5′ terminus and a NotI site and a Flag sequence at the 3′ terminus. The HindIII–NotI fragments of *ALK* cDNA were subcloned into pcDNA3 to generate expression plasmids. After resequencing to confirm that they had no other mutations, the *ALK* plasmids were used for transfection into NIH3T3 cells using Effectene Transfection Reagent (Qiagen) according to the suggested manufacturer's protocol. The transfected NIH3T3 cells were selected in 800 $\mu g\ ml^{-1}$ G418 for 2 weeks to obtain stably expressing clones.

To evaluate the phosphorylation status of ALK mutants, the cell lysates of stable clones were immunoprecipitated with antibodies to Flag (Sigma) and the resulting precipitates were subjected to western blot analysis with the antibody specific to pTyr1604 (Cell Signaling Technology) of ALK and the generic anti-phosphotyrosine antibody (PY20). The *in vitro* kinase activity of ALK mutants was measured using a non-radioactive isotope solid-phase enzyme-linked immunosorbent assay using the Universal Tyrosine Kinase Assay kit (Takara) according to the manufacturer's suggested protocol. We also performed the *in vitro* kinase assay with the synthetic YFF peptide (Operon Biotechnologies) as described previously[18]. For anchorage-independent growth analysis, 1×10^3 stably transfected NIH3T3 cells were mixed in 0.3% agarose with 10% FBS-DMEM and plated on 0.6% agarose-coated 35-mm dishes. After culture for 28 days, the colonies of >0.1 mm in diameter were counted. The quantification of the colonies was from three independent experiments. To investigate the downstream signalling of ALK, western blot analysis was performed using the anti-ERK1/2, anti-phospho-ERK1/2, anti-AKT, anti-phospho-AKT, anti-STAT3 and anti-phospho-STAT3 antibodies (Cell Signaling Technology)[15].

The cDNA mutant of *ALK* was also inserted into the pMXS plasmid and the constructs were introduced into NIH3T3 cells by the calcium phosphate method as described previously[9]. The cells were then either cultured for 21 days or injected subcutaneously at six sites in three nude mice.

Inhibition of ALK through RNAi-mediated knockdown. To suppress the expression of the ALK protein, two different pairs of *ALK* siRNAs (*ALK* siRNA1 and *ALK* siRNA2) were obtained (Qiagen)[15]. The sequences were 5′-GAGUCUGGCAGUUGACUUCdTdT-3′ for *ALK* siRNA1 and 5′-GCUCCGGCGUGCCAAGCAGdTdT-3′ for *ALK* siRNA2. A siRNA, targeting a sequence in firefly (*Photinus pyralis*) luciferase mRNA (*luc* siRNA), was used as a negative control (Qiagen)[15]. The sequences of *luc* siRNA were as follow: sense 5′-CGUACGCGGAAUACUUCGAdTdT-3′ and antisense 5′-UCGAAGUAUUCCGCGUACGdTdT-3′. Gene knockdown was achieved in SK-N-SH and LAN-2 cells using HiPerFect transfection reagent following the manufacturer's suggested instructions (Qiagen). To assess the effect of ALK knockdown on cell growth, these cells were seeded in 96-well plates at a concentration of 8.0×10^3 cells per well 24 h before transfection and assayed using the Cell Counting Kit-8 (Wako).

Statistical analysis. The significance of the correlation between *MYCN* amplification and *ALK* mutation was tested according to the conventional 2×2 contingency table using Fisher's exact test. The significance of the differences in kinase activity between wild-type and mutant ALK kinases was examined by the Mann–Whitney *U*-test based on the measured percentage activity of kinases in the precipitates of the corresponding samples. The significance of the differences in colony formation between wild-type and mutant ALK kinases was also examined by the Mann–Whitney *U*-test. The size of the hazards from possible risk factors, including International Neuroblastoma Staging System stages, *MYCN* status and *ALK* mutation/amplification were estimated by Cox regression analysis assuming a proportional hazard model using Stata software. Correlation between ploidy and clinical stage was tested by nptrend test.

23. Smith, E. I., Haase, G. M., Seeger, R. C. & Brodeur, G. M. A surgical perspective on the current staging in neuroblastoma—the International Neuroblastoma Staging System proposal. *J. Pediatr. Surg.* **24**, 386–390 (1989).
24. Takita, J. *et al.* Allelotype of neuroblastoma. *Oncogene* **11**, 1829–1834 (1995).
25. Takita, J. *et al.* Absent or reduced expression of the caspase 8 gene occurs frequently in neuroblastoma, but not commonly in Ewing sarcoma or rhabdomyosarcoma. *Med. Pediatr. Oncol.* **35**, 541–543 (2000).
26. Takita, J. *et al.* Allelic imbalance on chromosome 2q and alterations of the caspase 8 gene in neuroblastoma. *Oncogene* **20**, 4424–4432 (2001).

19. N. Loeuille, M. Loreau, *Proc. Natl. Acad. Sci. U.S.A.* **102**, 5761 (2005).
20. A. G. Rossberg, H. Matsuda, T. Amemiya, K. Itoh, *Ecol. Complex.* **2**, 312 (2005).
21. A. G. Rossberg, H. Matsuda, T. Amemiya, K. Itoh, *J. Theor. Biol.* **241**, 552 (2006).
22. N. D. Martinez, L. J. Cushing, in *Ecological Networks: Linking Structure to Dynamics in Food Webs* (Oxford Univ. Press, Oxford, 2006), Box A, p. 87.
23. L.-F. Bersier, M.-F. Cattin, C. Banasek-Richter, R. Baltensperger, J.-P. Gabriel, in *Ecological Networks: Linking Structure to Dynamics in Food Webs* (Oxford Univ. Press, Oxford, 2006), Box B, p. 91.
24. Details of the model are given in *Science* Online.
25. P. Jordano, J. Bascompte, J. M. Olesen, *Ecol. Lett.* **6**, 69 (2003).
26. D. P. Vazquez, *Oikos* **108**, 421 (2005).
27. L. Santamaría, M. A. Rodríguez-Gironés, *PLoS Biol.* **5**, e31 (2007).
28. M. G. Neubert, S. C. Blumenshine, T. Jonsson, B. Rashleigh, *Oecologia* **123**, 241 (2000).
29. C. A. Layman, K. O. Winemiller, D. A. Arrington, D. B. Jepsen, *Ecology* **86**, 2530 (2005).
30. T. Jonsson, J. E. Cohen, S. R. Carpenter, *Adv. Ecol. Res* **36**, 1 (2005).
31. We thank The Center for the Study of Complex Systems at the University of Michigan for computational resources, Andy Dobson and two anonymous reviewers for insightful comments, and Café Ambrosia for a comfortable meeting place. This work was supported by a Centennial Fellowship of the James S. McDonnell Foundation to M.P.

Supporting Online Material

www.sciencemag.org/cgi/content/full/320/5876/658/DC1
Materials and Methods
Figs. S1 to S13
Tables S1 to S8
References

8 February 2008; accepted 27 March 2008
10.1126/science.1156269

ROS-Generating Mitochondrial DNA Mutations Can Regulate Tumor Cell Metastasis

Kaori Ishikawa,[1,2,3]* Keizo Takenaga,[4,5]* Miho Akimoto,[5] Nobuko Koshikawa,[4] Aya Yamaguchi,[1] Hirotake Imanishi,[1] Kazuto Nakada,[1,2] Yoshio Honma,[5] Jun-Ichi Hayashi[1]†

Mutations in mitochondrial DNA (mtDNA) occur at high frequency in human tumors, but whether these mutations alter tumor cell behavior has been unclear. We used cytoplasmic hybrid (cybrid) technology to replace the endogenous mtDNA in a mouse tumor cell line that was poorly metastatic with mtDNA from a cell line that was highly metastatic, and vice versa. Using assays of metastasis in mice, we found that the recipient tumor cells acquired the metastatic potential of the transferred mtDNA. The mtDNA conferring high metastatic potential contained G13997A and 13885insC mutations in the gene encoding NADH (reduced form of nicotinamide adenine dinucleotide) dehydrogenase subunit 6 (*ND6*). These mutations produced a deficiency in respiratory complex I activity and were associated with overproduction of reactive oxygen species (ROS). Pretreatment of the highly metastatic tumor cells with ROS scavengers suppressed their metastatic potential in mice. These results indicate that mtDNA mutations can contribute to tumor progression by enhancing the metastatic potential of tumor cells.

Because most chemical carcinogens bind preferentially to mitochondrial DNA (mtDNA) rather than to nuclear DNA (*1–3*), mtDNA is considered to be their major cellular target. It has been hypothesized that the resultant somatic mutations in mtDNA play a causal role in oncogenic transformation (*3*). Many subsequent studies have supported the idea of preferential accumulation of somatic mutations in tumor mtDNAs (*4–9*) and their contribution to tumor growth (*10*, *11*). However, the apparent high frequency of mtDNA mutations in tumors could be due either to their stochastic accumulation (*12*, *13*) or to laboratory errors (*14*). Moreover, if mtDNA mutations induce oncogenic transformation, all the offspring of a mother carrying such mutations should develop tumors due to the maternal inheritance of mtDNA (*15*, *16*), but no bias toward maternal inheritance of tumor development has been reported. Nonetheless, it remains possible that mtDNA mutations are involved at a later stage of tumorigenesis, for example, in the development of metastatic potential. Recent studies demonstrated that dysfunction of the tricarboxylic acid cycle (TCA cycle) caused by mutations in nuclear DNA controls tumor phenotypes by the induction of a pseudo-hypoxic pathway under normoxic conditions (*17–19*). However, there has been no evidence of the involvement of mtDNA mutations in the development of metastatic potential or in the regulation of the pseudo-hypoxic pathway because of the difficulty of excluding possible involvement of nuclear DNA mutations in these processes (*20*).

We have examined the role of pathogenic mtDNA mutations in the development of tumor cell metastasis by studying two mouse tumor cell lines with different metastatic potentials (low metastatic P29 and high metastatic A11 cells) that originated from Lewis lung carcinoma (table S1) (*21–23*). We compared mitochondrial respiratory function by estimating the activities of respiratory complexes and found that P29 cells had normal activities, whereas A11 cells showed reduced activity of complex I (NADH dehydrogenase) (Fig. 1A). Complex I defects were also observed in high metastatic fibrosarcoma B82M cells but not in high metastatic colon adenocarcinoma LuM1 cells (Fig. 1A), which suggests that metastatic tumors are not always associated with complex I defects.

Because complex I consists of subunits encoded by both nuclear DNA and mtDNA (*24*), it was necessary to determine which genome, nuclear or mitochondrial, was responsible for the complex I defects and whether the complex I defects were responsible for the high metastatic potential. We addressed these issues by complete reciprocal exchange of mtDNAs between P29 and A11 cells by means of cell fusion to isolate transmitochondrial cybrids (fig. S1A and table S2) and examined whether complex I defects and metastatic potentials were cotransferred with the mtDNA. The results showed that complex I activity decreased in the cybrids with A11 mtDNA, whereas those with P29 mtDNA showed normal activity, irrespective of whether their nuclear DNAs were derived from P29 or A11 cells (Fig. 1B). Thus, complex I defects in the cybrids with A11 mtDNA appear to result from pathogenic mutations in their mtDNA, not in their nuclear DNA. We then examined the metastatic potential of the cybrids by inoculating them into a tail vein (to test "experimental" metastasis) and under the skin (to test "spontaneous" metastasis) of C57BL/6 mice and counting the number of nodules formed in the lung. Cybrids with A11 mtDNA acquired high metastatic potential, whereas cybrids with P29 mtDNA lost metastatic potential (table S2). These observations suggest that complex I defects and high metastatic potential are transferred simultaneously with the transfer of mtDNA from the A11 cells, whereas normal complex I activity and low metastatic potential are transferred simultaneously with the transfer of mtDNA from P29 cells. The mtDNA of A11 cells is therefore likely to harbor a mutation(s) responsible for complex I defects and metastasis.

We next examined whether these findings could be generalized to additional tumor cell lines. In these experiments, we transferred mtDNA from A11 cells into fibrosarcoma B82 cells with low metastatic potential and normal complex I activity, resulting in isolation of B82mtA11 cybrids (table S2). Conversely, we transferred mtDNA from B82M cells, which are derived from B82 cells but express high metastatic potential and com-

[1]Graduate School of Life and Environmental Sciences, University of Tsukuba, 1-1-1 Tennodai, Tsukuba, Ibaraki 305-8572, Japan. [2]Tsukuba Advanced Research Alliance Center, University of Tsukuba, 1-1-1 Tennodai, Tsukuba, Ibaraki 305-8572, Japan. [3]Japan Society for the Promotion of Science (JSPS), 8 Ichiban-cho, Chiyoda-ku, Tokyo 102-8472, Japan. [4]Division of Chemotherapy, Chiba Cancer Center Research Institute, 666-2 Nitona, Chuo-ku, Chiba 260-8717, Japan. [5]Shimane University Faculty of Medicine, 89-1 Enya-cho, Izumo, Shimane 693-8501, Japan.

*These authors contributed equally to this work.
†To whom correspondence should be addressed. E-mail: jih45@sakura.cc.tsukuba.ac.jp

plex I defects, into low metastatic P29 cells, resulting in isolation of P29mtB82M cybrids. Both B82mtA11 and P29mtB82M cybrids acquired complex I defects (Fig. 1C) and high metastatic potential (table S2), which suggests the cotransfer of these phenotypes and the mtDNAs from high to low metastatic cells of different tumor types. Notably, transfer of mtDNA from high metastatic A11 and B82M cells into nontransformed NIH3T3 cells did not induce tumorigenicity and metastatic potential in the resultant NIHmtA11 and NIHmtB82M cybrids (fig. S2A and table S2). Thus, pathogenic mtDNA mutations that induce complex I defects are present in A11 and B82M cells and control development of metastases; however, these mutations do not control the development of tumorigenicity and metastasis, at least in nontransformed NIH3T3 cells.

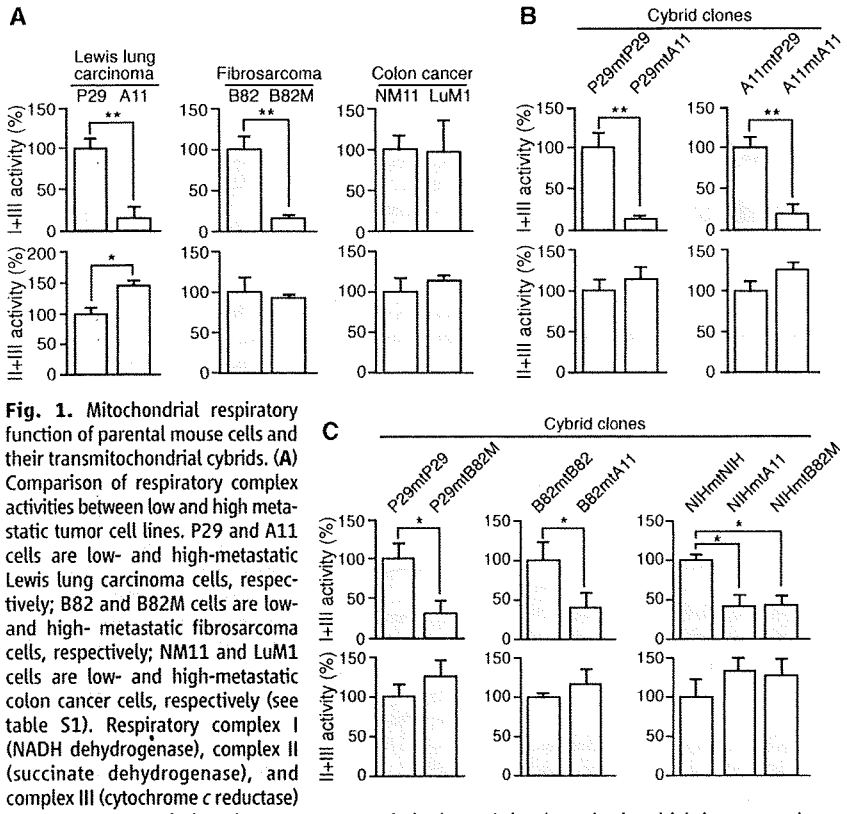

Fig. 1. Mitochondrial respiratory function of parental mouse cells and their transmitochondrial cybrids. **(A)** Comparison of respiratory complex activities between low and high metastatic tumor cell lines. P29 and A11 cells are low- and high-metastatic Lewis lung carcinoma cells, respectively; B82 and B82M cells are low- and high- metastatic fibrosarcoma cells, respectively; NM11 and LuM1 cells are low- and high-metastatic colon cancer cells, respectively (see table S1). Respiratory complex I (NADH dehydrogenase), complex II (succinate dehydrogenase), and complex III (cytochrome *c* reductase) are components of the electron-transport chain located in the mitochondrial inner membrane. Mitochondrial respiratory function was examined by estimating their activities. Because the activity of complexes II+III is normal in the A11 and B82M cells, the reduced activity of complexes I+III exclusively observed in the A11 and B82M cells should represent complex I defects. **(B)** Comparison of respiratory complex activities of the cybrids with mtDNA exchanged between low-metastatic P29 and high-metastatic A11 Lewis lung carcinoma cells. **(C)** Comparison of respiratory complex activities of the cybrids with mtDNA transferred from different types of tumor cells expressing high metastatic potential. Bars represent the mean ± SD ($n = 3$). *$P < 0.05$; **$P < 0.01$.

To identify the pathogenic mtDNA mutations that induced complex I defects and high metastatic potential in A11 and B82M cells, we compared the whole mtDNA sequences between P29 and A11 cells and between B82 and B82M cells. We conclude that a missense G13997A mutation in the A11 cells and a frame-shift 13885insC mutation in the B82M cells, both within the *ND6* (NADH dehydrogenase subunit 6) gene, are the pathogenic mutations that induce complex I defects, because these are the only mutations exclusively observed in the mtDNA of the high metastatic A11 cells and B82M cells (Table 1). Restriction enzyme digestion of the polymerase chain reaction products amplified using mismatched primers suggests complete and reciprocal replacement of parental mtDNAs in our cybrids (fig. S3).

We next explored how the mutated mtDNA and resultant complex I defects regulate metastasis. Because complex I defects may lead to overproduction of reactive oxygen species (ROS) (*24*, *25*), we estimated the amounts of ROS (fig. S4), and found that the cybrids with the mutated mtDNA from A11 cells showed enhanced ROS production, whereas the cybrids without the mutated mtDNA from P29 cells did not (fig. S4B). Such cotransfer of ROS-producing properties to the cybrids along with the transfer of mtDNA with or without the mutation suggests that ROS overproduction is due to the G13997A mutation. ROS overproduction was also observed in the P29mtB82M and B82mtA11 cybrids (fig. S4C).

How does ROS overproduction regulate metastasis, and which nuclear genes (if any) are involved in this process? We have reported previously (*22*, *26*) that A11 cells, but not P29 cells, show resistance to hypoxia-induced apoptosis, accompanied by up-regulation of antiapoptotic MCL-1 (myeloid cell leukemia–1). Moreover, A11 cells showed higher expression levels of two genes associated with neoangiogenesis, HIF-1α (hypoxia-inducible factor–1α) and VEGF (vascular endothelial growth factor), in comparison

Table 1. Identification of pathogenic mutations by comparison of mtDNA sequences between low- and high-metastatic mouse tumor cells.

Position	Gene	Amino acid change	Mouse strain	Cell lines					
			C57BL/6	P29	A11	L929	B82	B82M	NIH3T3
T6589C	*COI*	V421A	T	T	T	C	C	C	T
G9348A	*COIII*	V248I	G	G	G	A	A	A	G
T9461C	*ND3*	Silent	T	C	C	C	C	C	C
9821-PolyA	$tRNA^{Arg}$	–	8A	9A	9A	10A	10A	10A	10A
C11493A	*ND4*	P443T	C	A	A	C	C	C	C
A13672T	*ND6*	Silent	A	T	T	A	A	A	A
13885insC	*ND6*	Frame-shift	–	–	–	–	–	C*	–
G13997A	*ND6*	P25L	G	G	A*	G	G	G	G
Accession No.			AY172335	EU312160	EU312161	AJ489607	EU315229	EU315228	AY999076

*The G13997A mutation in *ND6* is a missense mutation that changes the amino acid proline to leucine at a site that is highly conserved throughout vertebrates. The 13885insC mutation in *ND6* is a frame-shift mutation that has been previously reported as a pathogenic mutation that induces substantial complex I defects in some sublines of an L929 fibroblast cell line and A9 cells (*23*).

with P29 cells (*27*). Thus, we focused here on the expression of these three nuclear-coded genes. We found that up-regulation of the MCL-1, HIF-1α, and VEGF was cotransferred when mutant mtDNA was transferred from A11 cells to the P29mtA11 and A11mtA11 cybrids. Down-regulation of three genes was cotransferred when wild-type mtDNA was transferred from P29 cells to the P29mtP29 and A11mtP29 cybrids (Fig. 2). Therefore, the mutated mtDNA and the resultant complex I defects induce up-regulation of the MCL-1, HIF-1α, and VEGF genes and are associated with high metastatic potential (fig. S1B). Gene expression profiling to compare P29mtP29 with P29mtA11 and A11mtP29 with A11mtA11 showed consistent up-regulation of other genes possibly related to metastasis in the cybrids with A11 mtDNA (table S3), which suggests involvement of additional genes in the mtDNA-mediated effects on metastasis.

To obtain direct evidence that ROS overproduction caused by the mutated mtDNA from A11 cells is responsible for high metastatic potential, we treated the P29mtA11 cybrids with ROS scavengers and examined their effects on the amounts of ROS and on the expression of the genes and the phenotypes related to metastasis. *N*-acetylcysteine (NAC), which has been used as an anticancer agent in preclinical models, was used as one ROS scavenger. The results showed that treatment of the cybrids with NAC in cell culture reduced the amount of ROS (Fig. 3A) and down-regulated MCL-1 (Fig. 3B). Moreover, pretreatment of the cybrids with NAC reduced their metastatic potential in two mouse models (Fig. 3C). Similar results were obtained by treatment with another ROS scavenger, Ebselen, which is a mimic of glutathione peroxidase (Fig. 3). Thus, ROS overproduction caused by the mutated mtDNA induces a high metastatic potential, at least in part, by up-regulation of MCL-1. This idea is supported by the finding that down-regulation of MCL-1 in P29mtA11 cybrids by small interfering RNA also suppressed their metastatic potential (fig. S5). Moreover, NAC treatment suppressed the metastatic potential without reducing glycolytic activity (fig. S6), which suggests that metastasis is not caused by up-regulation of glycolysis.

Contribution of mtDNA to tumor cell metastasis can be extended to human tumors, because the transfer of mtDNA from human breast cancer MDA-MB-231 cells expressing high metastatic potential into low metastatic HeLa cells induces

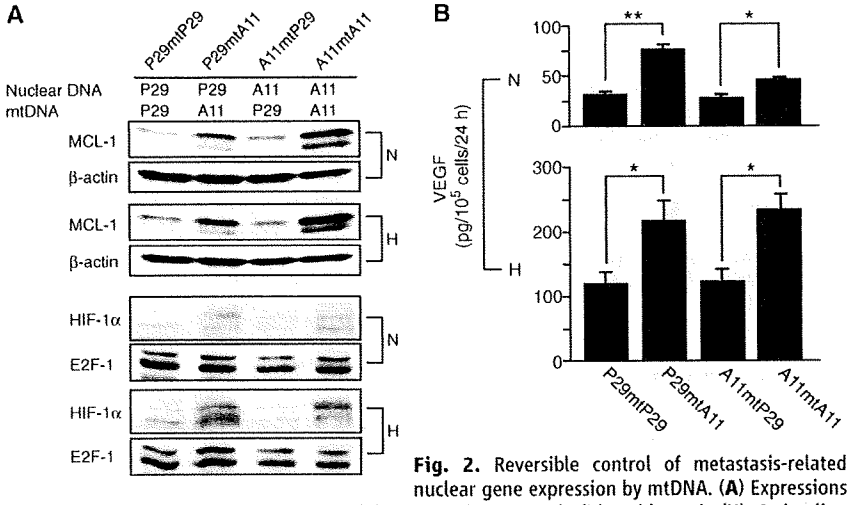

Fig. 2. Reversible control of metastasis-related nuclear gene expression by mtDNA. **(A)** Expressions of nuclear-coded MCL-1 and HIF-1α and **(B)** VEGF under normoxia (N) and hypoxia (H). As loading controls in the Western blots, we used β-actin for MCL-1 and E2F-1 for HIF-1α (A). In (B), blue bars represent cybrids carrying mtDNA from P29 cells (P29mtP29 and A11mtP29), and red bars represent cybrids carrying mtDNA from A11 cells (A11mtA11 and P29mtA11). Bars represent the mean ± SD (n = 3). *P < 0.01; **P < 0.001.

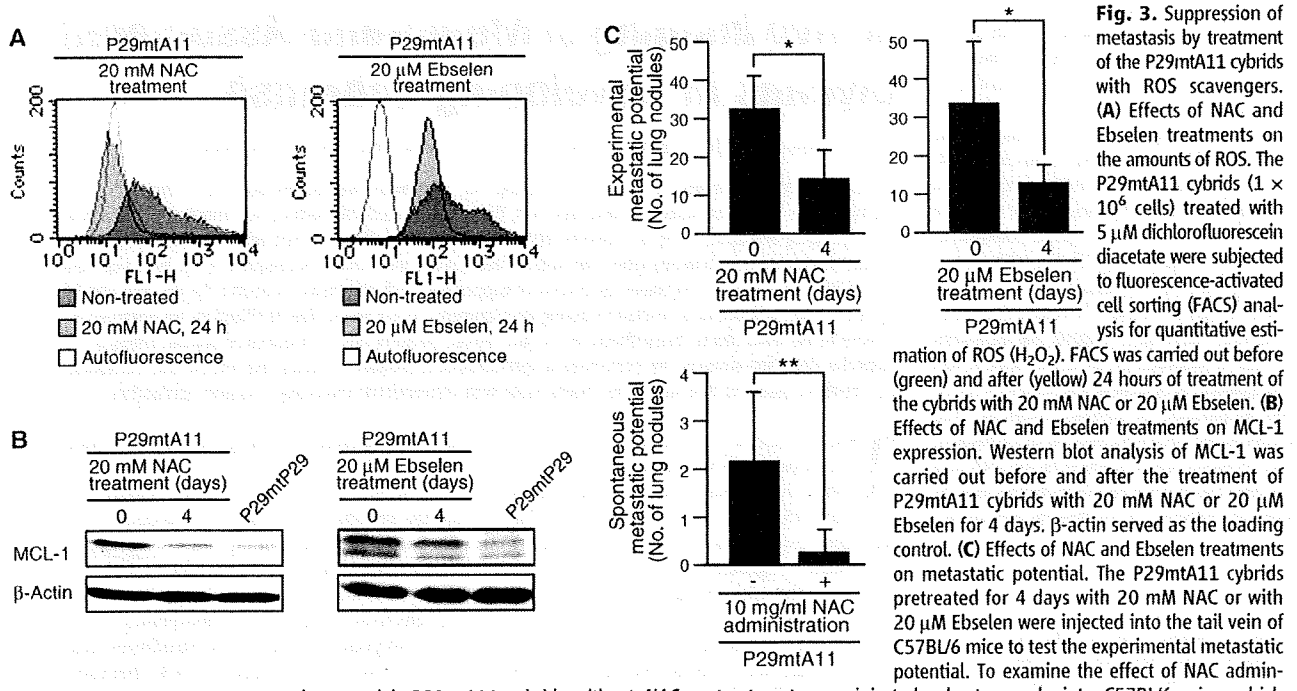

Fig. 3. Suppression of metastasis by treatment of the P29mtA11 cybrids with ROS scavengers. **(A)** Effects of NAC and Ebselen treatments on the amounts of ROS. The P29mtA11 cybrids (1 × 10^6 cells) treated with 5 μM dichlorofluorescein diacetate were subjected to fluorescence-activated cell sorting (FACS) analysis for quantitative estimation of ROS (H_2O_2). FACS was carried out before (green) and after (yellow) 24 hours of treatment of the cybrids with 20 mM NAC or 20 μM Ebselen. **(B)** Effects of NAC and Ebselen treatments on MCL-1 expression. Western blot analysis of MCL-1 was carried out before and after the treatment of P29mtA11 cybrids with 20 mM NAC or 20 μM Ebselen for 4 days. β-actin served as the loading control. **(C)** Effects of NAC and Ebselen treatments on metastatic potential. The P29mtA11 cybrids pretreated for 4 days with 20 mM NAC or with 20 μM Ebselen were injected into the tail vein of C57BL/6 mice to test the experimental metastatic potential. To examine the effect of NAC administration on spontaneous metastatic potential, P29mtA11 cybrids without NAC pretreatment were injected subcutaneously into C57BL/6 mice, which subsequently received 10 mg/ml NAC in drinking water ad libitum. Bars represent the mean ± SD (n = 6). *P < 0.05; **P < 0.01.

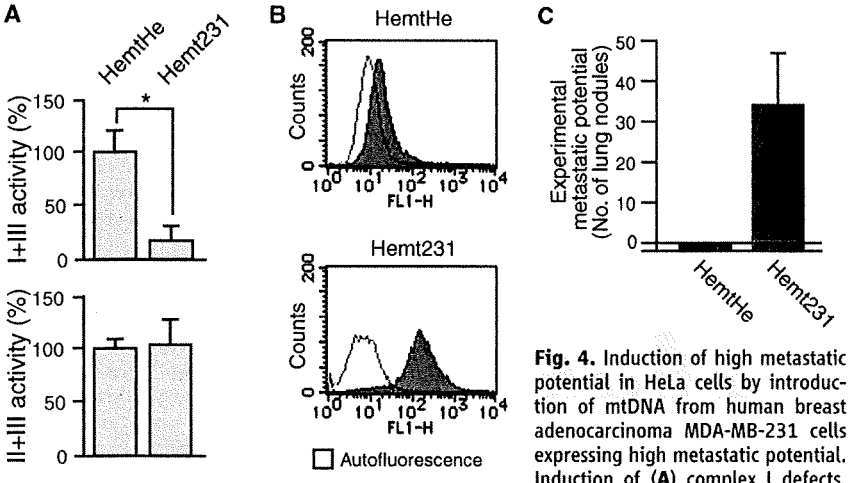

Fig. 4. Induction of high metastatic potential in HeLa cells by introduction of mtDNA from human breast adenocarcinoma MDA-MB-231 cells expressing high metastatic potential. Induction of **(A)** complex I defects, **(B)** ROS overproduction, and **(C)** high metastatic potential in the Hemt231 cybrids. HemtHe, HemtHe cybrids carrying nuclear DNA from ρ^0 HeLa cells and mtDNA from wild-type HeLa cells; Hemt231, Hemt231 cybrids carrying nuclear DNA from ρ^0 HeLa cells and mtDNA from MDA-MB-231 cells. Bars represent the mean ± SD (n = 5). *P < 0.05.

complex I defects, increased ROS production, and high metastatic potential in HeLa cells (Fig. 4). These observations suggest that the mtDNA in MDA-MB-231 cells can promote metastasis, although we have not done the mtDNA sequencing. Therefore, the metastatic potential of all the mouse and human tumor cell lines that we examined was greatly enhanced by exchanging their endogenous mtDNA with mutant mtDNA that induces complex I–mediated ROS overproduction. Recent reports showed that a pathogenic mutation in the *ATP6* gene of human mtDNA generated ROS and enhanced tumor growth (*10*, *11*). However, in our experiments, the enhanced growth rate of primary tumors did not necessarily correlate with expression of the high metastatic potential in mouse tumors (fig. S2B).

This study partially resolves the debate on the relevance of mtDNA mutations in tumors (*4*–*14*) by showing that mutations in mtDNA can control the metastatic potential of certain tumor cells but that they do not confer tumorigenic potential to nontransformed mouse NIH3T3 cells. Moreover, reversible regulation of metastasis by the exchange of mtDNA between P29 and A11 cells and by treatment with ROS scavengers suggests that metastasis of these cells is regulated by ROS-mediated reversible up-regulation of nuclear genes but not by ROS-mediated acceleration of genetic instability. The mtDNA-mediated reversible control of metastasis, therefore, reveals a novel function of mtDNA and suggests that in such cases ROS scavengers may be therapeutically effective in suppressing metastasis.

References and Notes

1. J. A. Allen, M. M. Coombs, *Nature* **287**, 244 (1980).
2. J. M. Backer, I. B. Weinstein, *Science* **209**, 297 (1980).
3. J. W. Shay, H. Werbin, *Mutat. Res.* **186**, 149 (1987).
4. K. Polyak *et al.*, *Nat. Genet.* **20**, 291 (1998).
5. M. S. Fliss *et al.*, *Science* **287**, 2017 (2000).
6. J. S. Penta, F. M. Johnson, J. T. Wachsman, W. C. Copeland, *Mutat. Res.* **488**, 119 (2001).
7. R. W. Taylor, D. M. Turnbull, *Nat. Rev. Genet.* **6**, 389 (2005).
8. A. M. Czarnecka, P. Golik, E. Bartnik, *J. Appl. Genet.* **47**, 67 (2006).
9. M. E. Gallardo *et al.*, *Hum. Mutat.* **27**, 575 (2006).
10. Y. Shidara *et al.*, *Cancer Res.* **65**, 1655 (2005).
11. J. A. Petros *et al.*, *Proc. Natl. Acad. Sci. U.S.A.* **102**, 719 (2005).
12. H. A. Coller *et al.*, *Nat. Genet.* **28**, 147 (2001).
13. R. W. Taylor *et al.*, *J. Clin. Invest.* **112**, 1351 (2003).
14. A. Salas *et al.*, *PLoS Med.* **2**, e296 (2005).
15. H. Kaneda *et al.*, *Proc. Natl. Acad. Sci. U.S.A.* **92**, 4542 (1995).
16. H. Shitara, J.-I. Hayashi, S. Takahama, H. Kaneda, H. Yonekawa, *Genetics* **148**, 851 (1998).
17. B. E. Baysal *et al.*, *Science* **287**, 848 (2000).
18. S. Niemann, U. Muller, *Nat. Genet.* **26**, 268 (2000).
19. E. Gottlieb, I. P. Tomlinson, *Nat. Rev. Cancer* **5**, 857 (2005).
20. L. H. Augenlicht, B. Heerdt, *Nat. Genet.* **28**, 104 (2001).
21. K. Takenaga, Y. Nakamura, S. Sakiyama, *Oncogene* **14**, 331 (1997).
22. M. Takasu, Y. Tada, J. O. Wang, M. Tagawa, K. Takenaga, *Clin. Exp. Metastasis* **17**, 409 (1999).
23. Materials and methods are available as supporting material on *Science* Online.
24. D. C. Wallace, *Science* **283**, 1482 (1999).
25. S. De Flora *et al.*, *Int. J. Cancer* **67**, 842 (1996).
26. N. Koshikawa, C. Maejima, K. Miyazaki, A. Nakagawara, K. Takenaga, *Oncogene* **25**, 917 (2006).
27. N. Koshikawa, A. Iyozumi, M. Gassmann, K. Takenaga, *Oncogene* **22**, 6717 (2003).

28. This work was supported by Grants-in-Aid for Scientific Research (S) from the Japan Society for Promotion of Science (JSPS), by Grants-in-Aid for Creative Scientific Research from JSPS, and by Grants-in-Aid for Scientific Research on Priority Areas from The Ministry of Education, Culture, Sports, Science and Technology of Japan (MEXT) to J.-I.H. This work was also supported by grants for a Research Fellowship from JSPS for Young Scientists to K.I. and by Grants-in-Aid for Third Term Comprehensive Control Research for Cancer from the Ministry of Health, Labour, and Welfare and for Scientific Research from MEXT to K.T. All animal experiments were performed in compliance with the institutional guidelines (Chiba Cancer Center and University of Tsukuba) for the care and use of laboratory animals.

Supporting Online Material

www.sciencemag.org/cgi/content/full/1156906/DC1
Materials and Methods
Figs. S1 to S6
Tables S1 to S3
References

25 February 2008; accepted 25 March 2008
Published online 3 April 2008;
10.1126/science.1156906
Include this information when citing this paper.

In Vivo Imaging of Membrane-Associated Glycans in Developing Zebrafish

Scott T. Laughlin,[1]* Jeremy M. Baskin,[1]* Sharon L. Amacher,[2] Carolyn R. Bertozzi[1,2,3,4]†

Glycans are attractive targets for molecular imaging but have been inaccessible because of their incompatibility with genetically encoded reporters. We demonstrated the noninvasive imaging of glycans in live developing zebrafish, using a chemical reporter strategy. Zebrafish embryos were treated with an unnatural sugar to metabolically label their cell-surface glycans with azides. Subsequently, the embryos were reacted with fluorophore conjugates by means of copper-free click chemistry, enabling the visualization of glycans in vivo at subcellular resolution during development. At 60 hours after fertilization, we observed an increase in de novo glycan biosynthesis in the jaw region, pectoral fins, and olfactory organs. Using a multicolor detection strategy, we performed a spatiotemporal analysis of glycan expression and trafficking and identified patterns that would be undetectable with conventional molecular imaging approaches.

The cell-surface glycome is a rich source of information that reports on the cell's physiological state. For example, changes in glycan structures serve as markers of altered gene expression during development (*1*) and disease progression (*2*). The dynamics of glycans at the plasma membrane reflect the activity of the cell's secretory machinery (*3*), and their relative abundances report on flux in metabolic pathways inside the cell (*4*). Glycans are therefore attractive targets for in vivo imaging but have been inaccessible because of their incompatibility with genetically encoded reporters (*5*).

To image glycans in vivo, we employed a strategy in which an azide is introduced into target biomolecules, priming them for selective covalent reaction with fluorescent probes (*5*). The azide is small, stable in biological systems, and selectively reactive with phosphines or activated alkynes. Previously, the Staudinger ligation (*6*, *7*) or copper-catalyzed click chemistry (*8*, *9*) have been used to detect azide-labeled biomolecules on cells ex vivo. However, in vivo

ERRATUM

Post date 18 July 2008

Reports: "ROS-generating mitochondrial DNA mutations can regulate tumor cell metastasis" by K. Ishikawa *et al.* (2 May, p. 661). The 25 February 2008 submission date was incorrect. The correct submission date was 10 September 2007.

Development 135, 1513-1524 (2008) doi:10.1242/dev.014340

Polycomb group proteins Ring1A/B are functionally linked to the core transcriptional regulatory circuitry to maintain ES cell identity

Mitsuhiro Endoh[1], Takaho A. Endo[2], Tamie Endoh[1], Yu-ichi Fujimura[1], Osamu Ohara[1], Tetsuro Toyoda[2], Arie P. Otte[3], Masaki Okano[4], Neil Brockdorff[5], Miguel Vidal[1,6] and Haruhiko Koseki[1,*]

The Polycomb group (PcG) proteins mediate heritable silencing of developmental regulators in metazoans, participating in one of two distinct multimeric protein complexes, the Polycomb repressive complexes 1 (PRC1) and 2 (PRC2). Although PRC2 has been shown to share target genes with the core transcription network, including Oct3/4, to maintain embryonic stem (ES) cells, it is still unclear whether PcG proteins and the core transcription network are functionally linked. Here, we identify an essential role for the core PRC1 components Ring1A/B in repressing developmental regulators in mouse ES cells and, thereby, in maintaining ES cell identity. A significant proportion of the PRC1 target genes are also repressed by Oct3/4. We demonstrate that engagement of PRC1 at target genes is Oct3/4-dependent, whereas engagement of Oct3/4 is PRC1-independent. Moreover, upon differentiation induced by Gata6 expression, most of the Ring1A/B target genes are derepressed and the binding of Ring1A/B to their target loci is also decreased. Collectively, these results indicate that Ring1A/B-mediated Polycomb silencing functions downstream of the core transcriptional regulatory circuitry to maintain ES cell identity.

KEY WORDS: Polycomb, Oct3/4 (Pou5f1), Gata6, ES cells, Chromatin, Silencing, Ring1A/B (Ring1/Rnf2), Mouse

INTRODUCTION

Embryonic stem (ES) cells derived from the inner cell mass (ICM) of mammalian blastocyst-stage embryos have unlimited growth potential while maintaining pluripotency – the ability to differentiate into all tissue types except the placenta (Evans and Kaufman, 1981; Martin, 1981). These properties of ES cells are maintained by symmetrical self-renewal, producing two identical stem cell daughters upon cell division (Burdon et al., 2002). The maintenance of ES cell pluripotency is thought to involve a transcriptional regulatory hierarchy including the transcription factors Oct3/4 (Pou5f1 – Mouse Genome Informatics), Sox2 and Nanog, which may be central components judging by their unique expression patterns and essential roles during early murine development (Avilion et al., 2003; Chambers et al., 2003; Mitsui et al., 2003; Nichols et al., 1998).

Recent genome-wide chromatin immunoprecipitation (ChIP) analyses revealed that OCT4, SOX2 and NANOG co-occupy the promoters of a large group of genes in human ES cells (Boyer et al., 2005), suggesting that these factors form a core regulatory feedback circuit, in which all three factors regulate the expression of themselves as well as of each other (Catena et al., 2004; Kuroda et al., 2005; Okumura-Nakanishi et al., 2005; Rodda et al., 2005). This positive-feedback loop promotes self-renewal of pluripotent ES cells by repressing transcription factors involved in differentiation and development, whilst likely activating the expression of genes involved in ES cell maintenance (Boyer et al., 2005).

The execution of differentiation programs in ES cells is likely to be preceded by interruption of the positive-feedback loop by developmental regulators such as Cdx2 and Gata6. The expression of Cdx2 and Gata6 is repressed by Oct3/4 and Nanog in undifferentiated ES cells (Boyer et al., 2005; Loh et al., 2006; Mitsui et al., 2003; Niwa et al., 2000; Niwa et al., 2005), and the enforced expression of Cdx2 and Gata6 quickly shuts down the positive loop and promotes a rapid transition from the undifferentiated to the differentiated state (Fujikura et al., 2002; Niwa et al., 2005). Therefore, the positive-feedback loops and developmental regulators are reciprocally engaged to maintain ES cell identity; however, the molecular mechanisms underlying this reciprocal interaction are not fully understood.

The Polycomb group (PcG) of proteins mediate heritable silencing of developmental regulators in metazoans, participating in one of two distinct multimeric protein complexes, the Polycomb repressive complexes 1 (PRC1) and 2 (PRC2) (Cao et al., 2002; Czermin et al., 2002; Kuzmichev et al., 2002; Muller et al., 2002; Shao et al., 1999). In mammals, the core PRC2 is composed of Eed, Ezh2 and Suz12 and catalyses trimethylation of histone H3 at lysine 27 (H3K27), which in turn is thought to provide a recruitment site for PRC1 (Cao et al., 2002; Czermin et al., 2002; Fischle et al., 2003; Kuzmichev et al., 2002; Min et al., 2003). The core PRC1 is composed of orthologs of *Drosophila* Polycomb (Cbx2, Cbx4 and Cbx8), Posterior sex combs [Mel18 (Pcgf2) and Bmi1], Sex comb extra (Ring1A and Ring1B, also known as Ring1 and Rnf2, respectively – Mouse Genome Informatics) and Polyhomeotic (Phc1, Phc2 and Phc3). Recent studies demonstrate that mono-ubiquitylation of histone H2A at lysine 119 is important in PcG-mediated silencing, with Ring1A/B functioning as the E3 ligase in this reaction (de Napoles et al., 2004; Wang et al., 2004).

[1]RIKEN Research Center for Allergy and Immunology, and [2]RIKEN Genomic Sciences Center, 1-7-22 Suehiro, Tsurumi-ku, Yokohama 230-0045, Japan. [3]Swammerdam Institute for Life Sciences, University of Amsterdam, Kruislaan 406, 1098 SM Amsterdam, The Netherlands. [4]RIKEN Center for Developmental Biology, 2-2-3 Minatojima-minamimachi, Chuo-ku, Kobe, Hyogo 6500047, Japan. [5]Developmental Epigenetics Group, MRC Clinical Sciences Centre, ICFM, Hammersmith Hospital, DuCane Road, London W12 ONN, UK. [6]Centro de Investigaciones Biologicas, Department of Developmental and Cell Biology, Ramiro de Maeztu 9, 28040 Madrid, Spain.

*Author for correspondence (e-mail: koseki@rcai.riken.jp)

Accepted 29 January 2008

Mouse and human ES cells have recently been analyzed by genome-wide ChIP, and PRC1 and PRC2 have been shown to repress genes involved in processes including development, transcriptional regulation and morphogenesis, via direct interactions with target genes (Boyer et al., 2006; Lee et al., 2006). Notably, PRC2 has been shown to share target genes with OCT4, SOX2 and/or NANOG in human ES cells (Lee et al., 2006). However, it is still unclear whether PcG and the core transcription network are functionally linked to regulate expression of their target genes.

In this study, we addressed the role of PRC1 in mouse ES cell maintenance and its functional interaction with the core transcriptional regulatory circuitry. We find that PRC1 is essential for the maintenance of ES cell identity and for the repression of developmental regulators by inhibiting chromatin remodeling. We go on to show that Ring1A/B-mediated PcG silencing is Oct3/4-dependent, whereas it is abolished by developmental cues resulting in *Gata6* activation. Collectively, our data suggest that Ring1A/B-mediated Polycomb silencing functions downstream of the core transcriptional regulatory circuitry to maintain ES cell self-renewal.

MATERIALS AND METHODS

Mouse cells

Eed-KO, *Dnmt1*-KO, *Oct3/4* conditional KO (ZHBTc4) ES cell lines and the ES cell line expressing a Gata6-GR fusion (G6GR) were described previously (Azuara et al., 2006; Lei et al., 1996; Niwa et al., 2000; Shimosato et al., 2007). Generation of mutant *Ring1A* and *Ring1B* flox alleles were described previously (Cales et al., 2008; del Mar Lorente et al., 2000). *Rosa26::CreERT2* transgenic mice were purchased from Artemis Pharmaceuticals (Seibler et al., 2003). *Ring1A*$^{-/-}$;*Ring1B*$^{fl/fl}$;*Rosa26::CreERT2* ES cells were derived from blastocysts. Male ES cells were used in this study.

Immunoprecipitation (IP) and chromatin immunoprecipitation (ChIP) analyses

IP (Isono et al., 2005a) and ChIP (Orlando et al., 1997) were performed as previously described. Immunoprecipitated and input DNA were quantified by real-time PCR. Primer and probe sequences are available upon request. Antibodies used in this study are listed in Table 1.

Reverse transcription and quantitative real-time PCR

RNA extraction and cDNA synthesis were performed as described previously (Isono et al., 2005b). Quantitative real-time PCR was carried out using the SYBR Green (Stratagene, Agilent Technologies, Santa Clara, CA) or Taqman (Biosearch Technologies, Novato, CA) method and amplifications detected with an Mx3005P (Stratagene, La Jolla, CA). Primer and probe sequences are available upon request.

Microarray methods and data analysis

Total RNA was extracted using Trizol (Invitrogen, Carlsbad, CA) and purified with RNeasy separation columns (Qiagen, Hilden, Germany). First-strand cDNA was synthesized and hybridized to Affymetrix GeneChip Mouse Genome 430 2.0 arrays (Affymetrix, Santa Clara, CA) to assess and compare the overall gene expression profiles.

To obtain normalized intensities from at least two slides, the quantile normalization method was used for every feature on the array (Bolstad et al., 2003). We calculated the log of the ratio of intensity in the knockout (KO) samples to the intensity in the respective control samples. Probes were not applied for further analysis when signals were at insignificant levels in control and KO samples. The expression change of a gene was calculated using the geometric mean of all probes aligned on the gene.

The microarray and ChIP-chip data are available in the NCBI Gene Expression Omnibus (GEO) under the series GSE10573 [NCBI GEO] with sample accession numbers GSM265040 to GSM265045, GSM266065 to GSM266067, GSM266076, GSM266077, GSM266115, GSM266837 and GSM266838.

Comparable expression analyses between KO ES cells

We obtained Pearson product-moment correlation coefficients of the logarithms of expression changes between respective KO ES cells. The 95% confidence intervals of correlation coefficients were calculated using Z transformation. Eigenvalues and eigenvectors of the distribution in scatter diagrams were calculated using principal component analysis with software R (http://www.r-project.org/).

Gene ontology (GO) analysis

We performed GO analysis using our in-house programs written in Python and C++ and GO data retrieved from the Gene Ontology database (http://www.geneontology.org), KEGG (http://www.genome.jp/kegg/) and others (Auernhammer and Melmed, 2000; Heinrich et al., 2003). The version of the dataset used was Oct 27th, 2006, submitted by Mouse Genome Informatics (MGI). We aligned microarray probes on mouse genes and assigned GO terms on all probes using these alignments. The significance of each GO term was determined using Fisher's exact test and Bonferroni adjustment for multiple testing. The *P*-value reflects the likelihood that we would observe such enrichment or higher by chance. Subsequent statistical examinations were also conducted using Fisher's exact test.

ChIP-chip experiment, assignment of IP regions and calculation of fold enrichment

ChIP-on-chip analysis of Ring1B binding was carried out using the Mouse Promoter ChIP-on-chip Microarray Set (G4490A; Agilent Technologies). ES cells were subjected to ChIP assay using anti-Ring1B antibody as described (Fujimura et al., 2006). Purified immunoprecipitated and input DNA were subjected to blunt ligation with linker oligo DNA, linker-

Table 1. Antibodies used in this study

Target protein	Species and clonality	Experiment	Source/reference
Oct3/4	Mouse monoclonal (C-10)	WB, IP	Santa Cruz (sc-5279)
Oct3/4	Goat polyclonal	ChIP	Santa Cruz (sc-8628X)
Ring1B	Mouse monoclonal (#3)	WB, IP, ChIP	(Atsuta et al., 2001)
Phc1	Mouse monoclonal	WB, ChIP	(Miyagishima et al., 2003)
Mel18	Goat polyclonal	WB	Abcam (ab5267)
Cbx2	Mouse monoclonal (2C6)	WB	(Fujimura et al., 2006)
Rybp	Rabbit polyclonal	WB	(Garcia et al., 1999)
Eed	Mouse monoclonal (M26)	WB, ChIP	(Hamer et al., 2002)
Suz12	Mouse monoclonal (4F7)	WB	Made in our laboratory
Ezh2	Mouse monoclonal (M10)	WB	(Hamer et al., 2002)
Acetylated histone H3	Rabbit polyclonal	WB, ChIP	Millipore/Upstate (06-599)
Trimethylated histone H3-K4	Rabbit polyclonal	WB, ChIP	Millipore/Upstate (07-473)
Trimethylated histone H3-K27	Rabbit polyclonal	WB, ChIP	Millipore/Upstate (07-449)
Ubiquitylated histone H2A	Mouse monoclonal (E6C5)	WB	Millipore/Upstate (05-678)
RNA polymerase II	Mouse monoclonal (8WG16)	ChIP	Millipore/Upstate (05-952)
Lamin B	Goat polyclonal	WB	Santa Cruz (sc-6216)

WB, western blot; IP, immunoprecipitation; ChIP, chromatin immunoprecipitation.

mediated PCR (LM-PCR), labeling, hybridization and washing following the Agilent mammalian ChIP-on-chip protocol. Scanned images were quantified with Agilent Feature Extraction software under standard conditions.

Assignment of regions bound by Ring1B around transcription start sites (TSSs) was carried out using direct sequence alignment on the mouse genome database (NCBI version 36). The location of Ring1B-bound regions was compared with a set of transcripts derived from the MGI database. We assigned bound regions that were within –8 kb to +2 kb of the TSS. Alignments on mouse genome and TSSs of genes were retrieved from Ensembl (http://www.ensembl.org).

The measured intensity ratios (IP/input: fold enrichment) were calculated, and the maximum value of the ratios in each promoter region (–8 kb to +2 kb around TSS) of a gene was used to represent the fold enrichment of the gene. Fold enrichment was calculated only for probes whose signals both from IP and input DNAs were significant ($P<10^{-3}$).

RESULTS

Ring1A/B are required for the maintenance of ES cell identity

To investigate the role of PRC1 for maintenance of mouse ES cell identity, it was necessary to generate *Ring1A/B* double-knockout (dKO) ES cells because *Ring1B* single-knockout (*Ring1B*-KO) ES cells can be cultured for >20 passages and exhibit ES cell morphology (de Napoles et al., 2004; Fujimura et al., 2006) (data not shown). Thus, we established *Ring1A*$^{-/-}$;*Ring1B*$^{fl/fl}$; *Rosa26*::*CreERT2* ES cell lines, in which *Ring1B* could be conditionally deleted by 4-hydroxy tamoxifen (OHT) treatment. Ring1B protein levels were dramatically depleted within 48 hours of OHT administration (Fig. 1A), and loss of Ring1B resulted in reduced levels of other PRC1 components Mel18, Phc1/2 and Cbx2 (Fujimura et al., 2006; Leeb and Wutz, 2007). At a global level, PRC1-regulated mono-ubiquitylated histone H2A (H2Aub1) was rapidly depleted within 48 hours following OHT treatment (Fig. 1B). We thus concluded that PRC1 could be conditionally depleted in this ES cell line by OHT.

In the *Ring1A/B*-dKO, in contrast to the *Ring1B*-KO ES cells, proliferation was halted and the cells gradually lost typical ES cell morphology after OHT administration (Fig. 1C). Moreover, genome-wide mRNA analysis revealed preferential derepression of genes involved in differentiation and/or developmental processes (Fig. 1D; see also Table S1 in the supplementary material). These observations, considered together with structural and biochemical similarities of Ring1A and Ring1B (Buchwald et al., 2006), led us to hypothesize a compensatory role of Ring1A for Ring1B in the repression of developmental genes in ES cells. This idea is partly supported by the increased expression of Ring1A protein observed in the *Ring1B*-KO ES cells (see Fig. S1 in the supplementary material). We first compared gene expression between the *Ring1A/B*-dKO and *Ring1B*-KO ES cells by microarray analyses. We found that 491 genes were derepressed more than 2-fold in *Ring1B*-KO (constitutive), whereas in *Ring1A/B*-dKO (day 4) ES cells, 999 genes were derepressed (see Table S2 in the supplementary material). Fold expression changes for respective probes in *Ring1A/B*-dKO and *Ring1B*-KO ES cells, determined against the parental or wild-type cells, were plotted on a scatter diagram and the correlation was calculated according to Pearson (see Fig. S2 in the supplementary material). We found a strong correlation (r=0.386) in total calculable genes (see Fig. S2 in the supplementary material). This result indicates significant overlap of genes derepressed in *Ring1A/B*-dKO and *Ring1B*-KO ES cells. The level of derepression was much higher in *Ring1A/B*-dKO than in *Ring1B*-KO ES cells, as represented by differences in variance (see Fig. S2 in the supplementary material). On average, developmental genes were 1.389-fold derepressed in *Ring1A/B*-dKO ES cells, but 1.046-fold in *Ring1B*-KO (see Table S3 in the supplementary material). We confirmed these quantitative differences by evaluating the expression levels of several developmental regulators including *Gata6* and *Cdx2* by quantitative RT-PCR. These genes were significantly derepressed by conditional depletion of Ring1B, but the degree of derepression was higher in the *Ring1A/B*-dKO than in the *Ring1B*-KO cells (Fig. 1E). Therefore, Ring1A and Ring1B appear to act in a compensatory manner to repress the expression of developmental regulators in ES cells and consequently contribute to the maintenance of ES cells in an undifferentiated state. The phenotypic differences between *Ring1B*-KO and *Ring1A/B*-dKO ES cells are likely to be due to exaggerated derepression of developmental regulators such as *Gata6* and *Cdx2* in the dKO cells.

We next examined whether the derepression of developmental regulators is accompanied by disruption of the core transcriptional regulatory circuitry in ES cells. We performed multicolor immunofluorescence analysis for Oct3/4 and for Gata4, which is also expressed in primitive endoderm. Oct3/4 was expressed relatively uniformly in all of the control cells and Gata4 was also expressed in most of the cells (Fig. 1F, upper panels). Four days after OHT administration, we found striking heterogeneity in Oct3/4 expression (Fig. 1F, lower panels). In the example illustrated, most of the cells are compacted; however, a subset of cells at the edge spread out from the colony and exhibit epithelial cell morphology. Most of these cells expressed Gata4 but not Oct3/4 (Fig. 1F, arrowheads in lower right panel), which is likely to be indicative of the onset of spontaneous differentiation. Taken together with the gene expression analysis, these results indicate that Ring1A/B contribute crucially to the repression of ES cell differentiation and therefore to the maintenance of ES cell identity.

Ring1A/B mediate repression of developmental regulators by inhibiting chromatin remodeling via direct binding

We next used ChIP analysis to determine whether genes derepressed in *Ring1A/B*-dKO ES cells were direct targets of PRC1. As shown in Fig. 2A, we observed binding of Ring1B and Phc1, another component of PRC1, to *Hoxb8*, *Gata6*, *Cdx2*, *Zic1* and *T*, all of which are derepressed in the *Ring1A/B*-dKO (Fig. 1E). Binding to all these genes was significantly reduced 2 days after administration of OHT in *Ring1A*$^{-/-}$;*Ring1B*$^{fl/fl}$;*Rosa26*::*CreERT2* ES cells, suggesting that Ring1B is essential for the establishment of PRC1 at their respective loci.

We next examined whether genes derepressed in *Ring1A/B*-dKO ES cells were bound by Ring1B at their promoters using a ChIP-chip approach (Fig. 2B; see Tables S4 and S5 in the supplementary material). We identified almost the same set of Ring1B targets that had been reported previously, if a certain threshold is adopted to distinguish genes bound by Ring1B (Boyer et al., 2006) (data not shown). We further clarified linear correlations between the degree of Ring1B binding and derepression in *Ring1B*-KO and *Ring1A/B*-dKO ES cells (Fig. 2B). These results indicate that Ring1A/B generally repress transcription by directly binding to the target loci in a dose-dependent manner.

Recent studies have demonstrated that PcG targets in ES cells are often characterized by a unique chromatin configuration, being simultaneously enriched for histone modifications associated with gene activity [histone H3 lysine 4 trimethylation (H3K4me3) and lysine 9/14 acetylation (H3Ac)] and modifications associated with PcG-mediated repression [specifically H3K27 trimethylation

(H3K27me3)] (Azuara et al., 2006; Bernstein et al., 2006). With this in mind, we investigated changes in chromatin configuration upon Ring1A/B depletion. At a global level, PRC1-mediated H2Aub1 was rapidly depleted (Fig. 1B). By contrast, there was no detectable change in overall levels of either H3K4me3, H3Ac, H3K27me3 or PRC2 components (see Fig. S3 in the supplementary material). We then analyzed promoter regions of selected PcG target loci derepressed in *Ring1A/B*-dKO ES cells by ChIP. In addition to histone modifications, we analyzed binding of Eed and non-phosphorylated RNA polymerase II (RNAPII) (Fig. 2C). Levels of H3Ac, H3K4me3 and RNAPII binding were significantly increased, whereas those of Eed and H3K27me3 were decreased. Although the molecular mechanism for the decrease in Eed binding upon Ring1A/B depletion is unclear, it is possible that changes in chromatin structure caused by Ring1A/B depletion might secondarily affect Eed binding.

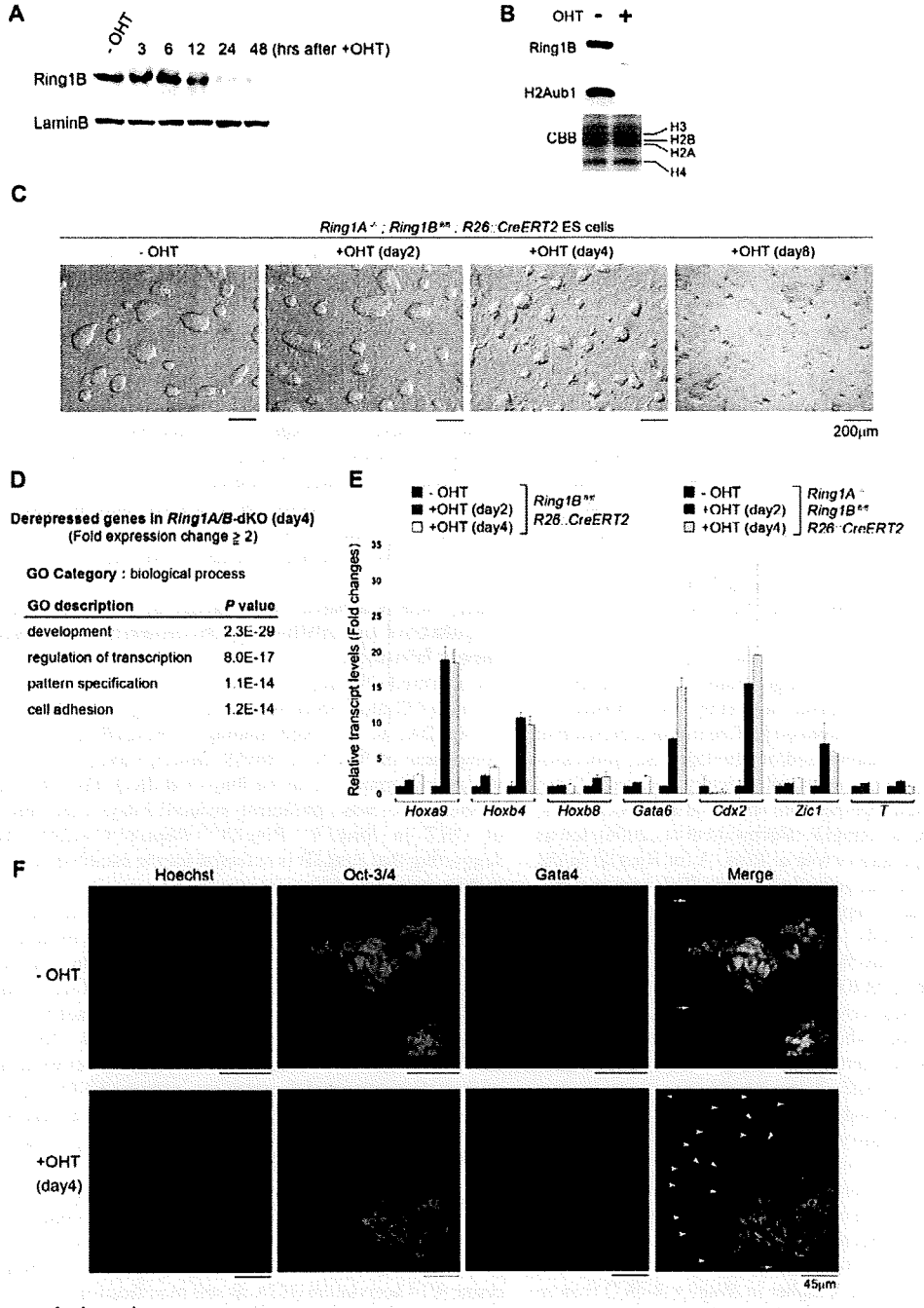

Fig. 1. See next page for legend.

Fig. 1. Ring1A/B are required for the maintenance of mouse ES cell identity. (**A**) Western blot analysis showing the kinetics of Ring1B depletion at 0, 3, 6, 12, 24 and 48 hours after treatment of *Ring1A*$^{-/-}$;*Ring1B*$^{fl/fl}$;*Rosa26*::*CreERT2* ES cells with 4-hydroxy tamoxifen (OHT). Lamin B served as a loading control. (**B**) Western blot showing Ring1B and mono-ubiquitylated H2A (H2Aub1) depletion 2 days after treatment with OHT in *Ring1A*$^{-/-}$;*Ring1B*$^{fl/fl}$;*Rosa26*::*CreERT2* ES cells. OHT was present in (+) or absent from (–) the ES cell culture medium. Coomassie Brilliant Blue (CBB) staining for histones was used as a loading control. (**C**) Morphology of conditional *Ring1A/B*-dKO ES cells. *Ring1A*$^{-/-}$;*Ring1B*$^{fl/fl}$;*Rosa26*::*CreERT2* ES cells were cultured in the absence (–OHT) or presence (+OHT) of OHT, which represent the single *Ring1A*-KO or *Ring1A/B*-dKO cells, respectively. At day 2, *Ring1A/B*-dKO ES cells retain ES-cell-like morphology; however, from day 3-4, *Ring1A/B*-dKO ES cells begin to lose ES-cell-like morphology. (**D**) Gene ontology (GO) analysis of genes more than 2-fold derepressed 4 days after OHT treatment of *Ring1A*$^{-/-}$;*Ring1B*$^{fl/fl}$;*Rosa26*::*CreERT2* ES cells. The significance (*P*-value) of the enrichment of each GO term is indicated for each category of biological process. For details, see Table S1 in the supplementary material. (**E**) Changes in expression levels of *Hoxa9*, *Hoxb4*, *Hoxb8*, *Gata6*, *Cdx2*, *Zic1* and *T* at 2 and 4 days after OHT treatment (+OHT) of *Ring1B*$^{fl/fl}$;*Rosa26*::*CreERT2* or *Ring1A*$^{-/-}$;*Ring1B*$^{fl/fl}$;*Rosa26*::*CreERT2* ES cells as determined by real-time PCR. Expression levels were normalized to an *Actb* control and are depicted as fold changes relative to the OHT-untreated (–OHT) ES cells. Error bars are based on the s.d. as derived from triplicate PCR reactions. (**F**) *Ring1A*$^{-/-}$;*Ring1B*$^{fl/fl}$;*Rosa26*::*CreERT2* ES cells were cultured in the absence (–OHT, upper panels) or presence (+OHT, day 4, lower panels) of OHT, and were immunostained with antibodies to Oct3/4 (green) and Gata4 (red). The left-most panels show nuclei stained with Hoechst 33342 (blue); the right-most panels show merged images. Arrowheads indicate differentiated cells that express Gata4 but not Oct3/4. Arrows indicate feeder cells. Scale bars: 200 μm in C; 45 μm in F.

The above results demonstrate that Ring1A/B depletion converts the local chromatin from an inactive into an active configuration. This would suggest that the engagement of PRC1 is important to ensure robust silencing within chromatin domains that are predisposed to transcriptional activation (Azuara et al., 2006; Bernstein et al., 2006).

A large number of genes are repressed by both Ring1A/B and Oct3/4

Given that Ring1A/B are required for the maintenance of ES cell identity, we next examined the relationship between Ring1A/B and the core transcriptional regulatory circuitry in ES cells, because a previous study demonstrated that OCT3/4, SOX2 and NANOG co-occupy a significant subset of PRC2 target genes in human ES cells (Lee et al., 2006). In fact, inactive genes bound by OCT3/4, SOX2 and/or NANOG in human ES cells are overrepresented among those genes more than 2-fold derepressed in *Ring1A/B*-dKO mouse ES cells (see Fig. S4 in the supplementary material).

To directly test whether Ring1A/B mediate transcriptional silencing by the core transcriptional circuitry we made use of *Oct3/4* conditional knockout ES cells (ZHBTc4) (Niwa et al., 2000), comparing changes in gene expression in *Oct3/4*-KO and *Ring1A/B*-dKO cells. Because most *Oct3/4*-KO ES cells begin to exhibit trophectoderm-like morphology within 2 to 3 days after induction (Niwa et al., 2000), we analyzed RNA from ES cells 1 day after tetracycline (Tc) treatment, at which time Oct3/4 protein is extensively depleted, thus minimizing the contribution of secondary changes in gene expression resulting from differentiation. As controls, we also analyzed gene expression in *Eed*- and *Dnmt1*-KO ES cells. *Dnmt1*-KO ES cells self-renew but fail to undergo differentiation upon induction (Lei et al., 1996). Fold changes for respective probes determined against the parental cells were distributed on scatter diagrams and the correlation among respective KO ES cells was calculated (Fig. 3A). We found a strong correlation in total calculable genes between *Oct3/4*-KO and *Ring1A/B*-dKO ES cells (r=0.279). Overall gene expression in *Ring1A/B*-dKO ES cells also exhibited a strong correlation (r=0.359) with the *Eed*-KO, which might represent functional engagement of PRC1 and PRC2. By contrast, we found no correlation of the *Dnmt1*-KO with either the *Ring1A/B*-dKO (r=0.078) or *Oct3/4*-KO (r=–0.001). This analysis indicates that a large number of genes in ES cells are concurrently repressed by Oct3/4 and Ring1A/B.

Next we tested which genes regulated by Oct3/4 and Ring1A/B are important in maintaining ES cell identity. For this purpose, we extended the comparative gene expression analysis into sorted genes based on GO term categories. We found a comparable correlation in genes involved in regulation of transcription, transcription, development and apoptosis (Fig. 3B). Notably, the highest correlation was seen in genes involved in signaling pathways for Notch and Lif, both of which are implicated in stem cell maintenance (Androutsellis-Theotokis et al., 2006; Williams et al., 1988).

To test whether this observed correlation is statistically significant, we investigated the average expression changes caused by Ring1A/B depletion in genes more than 2-fold derepressed and repressed by Oct3/4 depletion. We further estimated the correlation of the expression changes with the degree of Ring1B binding to the respective genes. On average, derepressed genes in *Oct3/4*-KO cells were significantly derepressed in the *Ring1A/B*-dKO, as represented by a value at the zero point on the x-axis (P=1.23×10^{-39}) (Fig. 3C, red circle; see also Table S6 in the supplementary material). The degree of derepression in *Ring1A/B*-dKO showed a linear correlation with the degree of Ring1B binding (Fig. 3C, red circles). Concordantly, 120 out of 670 genes repressed by Oct3/4 were bound by Ring1B (Fig. 3D). By contrast, repressed genes in the *Oct3/4*-KO were only slightly repressed in the *Ring1A/B*-dKO, and these were genes that bound less Ring1B, whereas this was not the case at genes bound by Ring1B at intermediate or high levels (Fig. 3C, blue circles). Taken together with the spontaneous differentiation observed in *Ring1A/B*-dKO ES cells, Ring1A/B appear to be functionally linked with Oct3/4 in mediating ES cell identity.

Oct3/4 is required to engage PRC1 and PRC2 at target gene promoters

To examine the molecular basis for the functional link between Oct3/4 and Ring1A/B, we used ChIP to investigate the effect of Oct3/4 deletion on the levels of Ring1B at selected targets bound by both Ring1B and Oct3/4 and/or Nanog (Boyer et al., 2005; Loh et al., 2006). Of the selected genes *Cdx2*, *Hand1*, *Gata6* and *Hoxb4* were derepressed 1 day after Oct3/4 depletion, whereas *T*, *Otx2* and *Hoxb8* were not (Fig. 4A). Ring1B binding was significantly reduced irrespective of transcriptional status, suggesting Oct3/4-mediated regulation Ring1B binding to the chromatin (Fig. 4B). We extended the analysis to examine whether this hierarchical link is applicable to other Ring1B target genes by the ChIP-chip approach. As shown in Fig. 4C, Ring1B binding to the promoter regions of the target genes was, on average, significantly reduced 2 days after Tc treatment of ZHBTc4 ES cells. Therefore, binding of Ring1B to the chromatin in ES cells is generally dependent on Oct3/4. It has

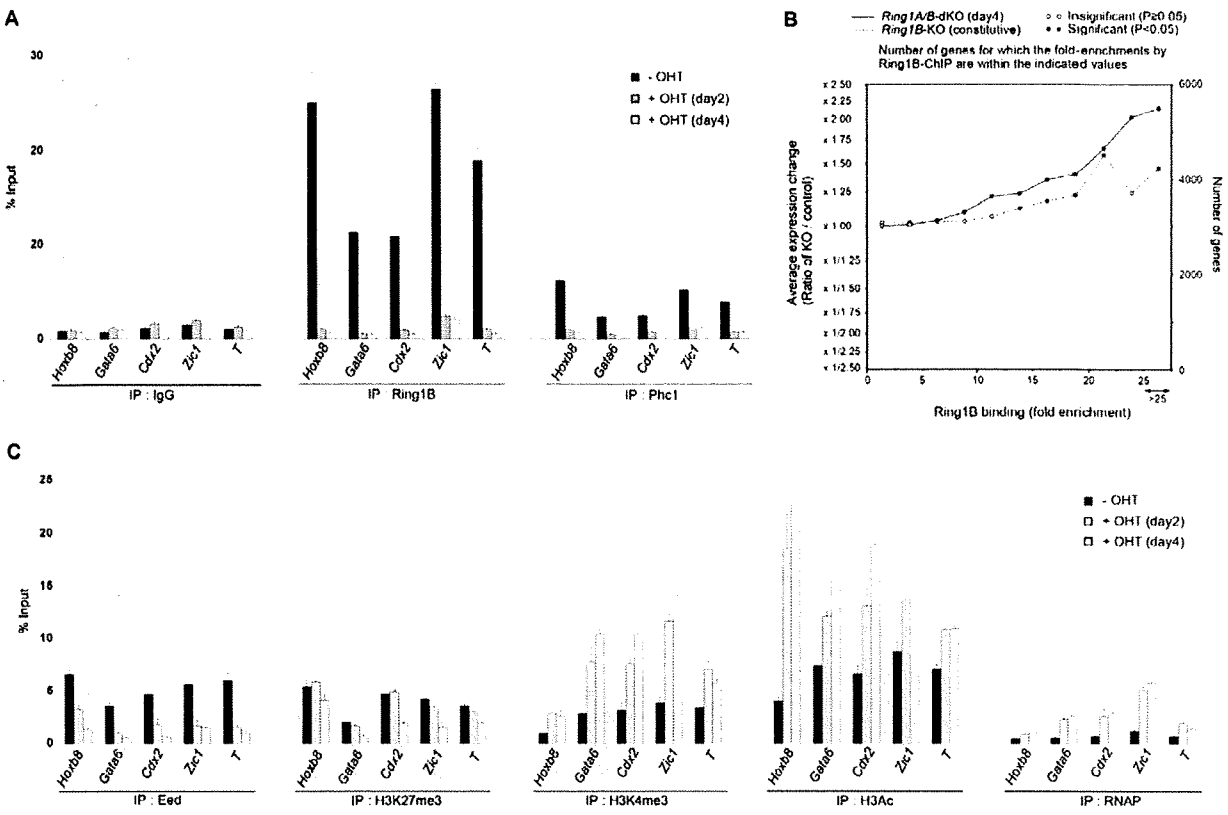

Fig. 2. Ring1A/B mediate repression of developmental regulators by inhibiting chromatin remodeling via direct binding. (**A**) Loss of Ring1B and Phc1 binding to the selected target promoter regions upon depletion of Ring1B in ES cells. Kinetics of local levels of Ring1B binding and Phc1 binding after OHT administration in *Ring1A*$^{-/-}$;*Ring1B*$^{fl/fl}$;*Rosa26*::*CreERT2* ES cells were determined by ChIP and site-specific real-time PCR. The relative amount of immunoprecipitated DNA is depicted as a percentage of input DNA. Error bars represent s.d. determined from at least three independent experiments. (**B**) Quantitative representation of the correlation between Ring1B binding and degree of derepression. Genes bound by Ring1B in their promoter regions in wild-type ES cells were identified by a ChIP-on-chip approach. Fold enrichment values for respective genes were calculated against the input and binned (each bin containing 2.5-fold enrichment). The number of genes in a bin (yellow bar) and the average change in expression from microarray analysis of *Ring1B*-KO (blue) and *Ring1A/B*-dKO (red) are indicated. Expression changes were statistically evaluated using Student's *t*-test under the null hypothesis that derepression was not observed. Significantly ($P<0.05$) derepressed bins and insignificant bins are indicated by solid and open circles, respectively. For actual values used to derive the graph and a list of Ring1B-bound genes, see Tables S4 and S5, respectively, in the supplementary material. (**C**) Changes in PRC2 binding and histone modification at Ring1B target loci following *Ring1A/B* depletion in ES cells. Kinetics of local levels of Eed, histone H3 lysine 27 trimethylation (H3K27me3), lysine 4 trimethylation (H3K4me3), lysine 9/14 acetylation (H3Ac), and non-phosphorylated RNA polymerase II (RNAPII) binding at the selected targets for Ring1B after OHT administration in *Ring1A*$^{-/-}$;*Ring1B*$^{fl/fl}$;*Rosa26*::*CreERT2* ES cells were determined by ChIP and site-specific real-time PCR. The relative amount of immunoprecipitated DNA is depicted as a percentage of input. Error bars represent s.d. determined from at least three independent experiments.

been reported that chromatin binding of Ring1B is also regulated by PRC2 functions (Boyer et al., 2006). We thus extended the analysis to address whether Oct3/4-dependent chromatin-binding of Ring1B involves PRC2, and found that binding of Eed to these genes was significantly reduced as well (Fig. 4B). Taken together, these results indicate that Oct3/4 mediates local engagement of PRC1 and PRC2.

Since enforced Ring1A/B depletion led to a rapid increase in the H3K4me3 level at the target genes (Fig. 2C), we next investigated changes in the degree of H3K4me3 at these genes upon Oct3/4 depletion. Notably, the level of H3K4me3 was increased at *Cdx2*, *Hand1*, *Gata6* and *Hoxb4*, whereas it was reduced or unchanged at *T*, *Otx2* and *Hoxb8*, consistent with increased gene expression (Fig. 4B). This indicates that the global reduction of PcG binding is not the sole mechanism for the changes in gene expression profile observed in ES cells upon Oct3/4 depletion. Oct3/4 has been suggested to upregulate some target genes and downregulate others. *Otx2* is one gene that has been experimentally verified to be upregulated directly by Oct3/4 (Boyer et al., 2005; Loh et al., 2006; Matoba et al., 2006). Moreover, the co-occupancy of promoters by PRC2 and OCT4/SOX2/NANOG has been demonstrated only at the transcriptionally repressed genes in human ES cells (Boyer et al., 2006). Considered together with the phenotypic difference between *Oct3/4*-KO and *Ring1A/B*-dKO ES cells, the global reduction in PcG binding might be a part of the mechanism for the differentiation of *Oct3/4*-KO ES cells.

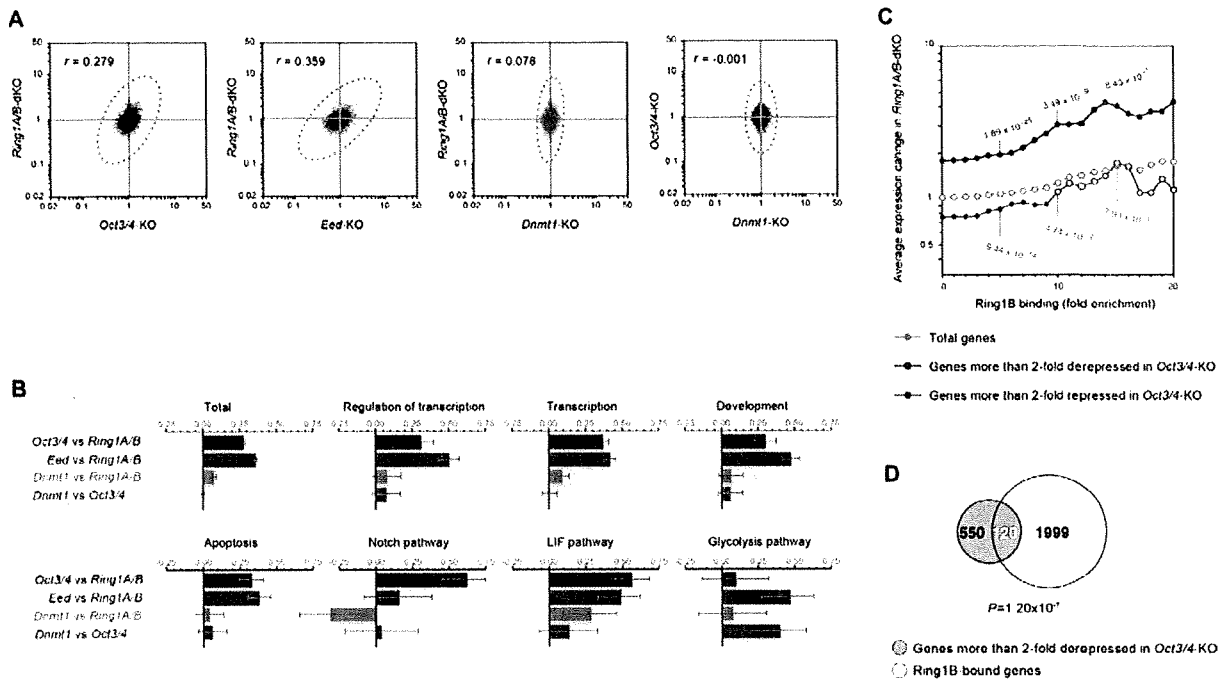

Fig. 3. Significant overlap of derepressed genes in *Ring1A/B*-dKO and *Oct3/4*-KO ES cells. (**A**) Scatter diagrams representing the correlation for changes in gene expression between respective KO ES cells. Each dot represents a specific probe. Fold changes of expression given by each probe in each KO against parental ES cells are dotted in the scatter diagram. Pearson's correlation coefficient (*r*) in each comparison is indicated in each panel. The distribution of dots is approximated by dotted ellipses. We prepared RNA from *Oct3/4*-KO ES cells 1 day after gene deletion was induced; *Ring1A/B*-dKO RNA was isolated at 4 days. Diagrams indicate the correlation of gene expression in *Eed*-KO versus *Ring1A/B*-dKO (green), *Oct3/4*-KO versus *Ring1AB*-dKO (red), *Dnmt1*-KO versus *Ring1A/B*-dKO (yellow), and *Dnmt1*-KO versus *Oct3/4*-KO (blue). (**B**) Pearson's correlation of expression changes for probes that belong to specific GO classifications are shown by bars. The same color codes are used as in A. Annotations are indicated above each graph. Error bars represent 95% confidence intervals of correlation coefficients calculated by Z transformation. (**C**) Graphical representation of correlation of derepressed genes in *Oct3/4*-KO and *Ring1A/B*-dKO ES cells in terms of the degree of Ring1B binding. Based on the genome-wide gene expression profiling, we first identified groups of genes more than 2-fold derepressed (red circles) or repressed (blue circles) in *Oct3/4*-KO ES cells. Average expression changes in *Ring1A/B*-dKO cells among those genes were plotted according to the degree of Ring1B binding determined by ChIP-chip and compared with the average of total genes (yellow circles). Where average expression changes in respective groups were statistically significant, relative to the total, the circles are solid; the open blue circles indicate that the difference from total genes is not statistically significant. *P*-values over 5-, 10- and 15-fold enrichment for Ring1B binding are shown. For actual values, see Table S6 in the supplementary material. (**D**) A significant fraction of the genes repressed by Oct3/4 is bound by Ring1B. The number of genes in each category of the Venn diagram is indicated.

Finally, we examined whether the binding of Oct3/4 depends on Ring1A/B. The levels of Oct3/4 binding to the PcG target sites were either unchanged or slightly decreased 2 to 4 days after OHT treatment of the *Ring1A/B*-dKO ES cells (Fig. 4D). Considering that the overall level of Oct3/4 decreases slightly 4 days after OHT treatment (see Fig. S3 in the supplementary material), we conclude that Ring1A/B are not directly required for the binding of Oct3/4 to the target sites.

In summary, loss of Oct3/4 consistently results in the reduction of Ring1B and Eed binding at PcG target genes in ES cells. Oct3/4 may maintain the repression of essential developmental regulators such as *Cdx2* and *Gata6* (Fujikura et al., 2002; Niwa et al., 2005) by maintaining local engagement of PRC1 and PRC2.

Molecular links between Polycomb and the core transcriptional regulatory circuitry

To determine the molecular mechanism for the global reduction of Ring1B binding upon Oct3/4 depletion, we investigated the effect of Oct3/4 deletion on the level of PRC1 and PRC2 proteins. Although Ring1B expression was only minimally affected during the first 48 hours of Tc treatment, expression of Phc1, Eed and Suz12 was significantly reduced (Fig. 5A). The decrease in Phc1 and PRC2 proteins was accompanied by a significant reduction in their respective transcript levels, whereas this was not the case for other PRC1 components, including *Ring1B* and *Bmi1* (Fig. 5B). Therefore, Oct3/4 regulates the expression of PRC1 and PRC2 components, and this may partly involve transcriptional regulation.

We also investigated whether the physical interaction of Ring1B with the Rex1 (Zfp42 – Mouse Genome Informatics) complex (Wang et al., 2006) could be extended to Oct3/4. Significant amounts of Oct3/4 and Ring1B as well as Rybp, a Ring1B-binding protein (Garcia et al., 1999), were found to form complexes in ES cells, whereas the PRC2 protein Suz12 did not co-immunoprecipitate with either Oct3/4 or Ring1B (Fig. 5C). Since reciprocal co-immunoprecipitation of Oct3/4 and Ring1B was not affected by the addition of ethidium bromide, which is known to

disrupt protein-DNA interactions without affecting protein-protein interactions (Lai and Herr, 1992) (Fig. 5C, right), this interaction is not mediated by genomic DNA. This result suggests that the local binding of PRC1 to chromatin might involve direct interactions between PRC1 and protein complexes that include Nanog and/or Oct3/4. Taken together, these results suggest that PRC1 is linked to the core transcriptional regulatory circuitry at multiple levels.

PRC1/2 binding is significantly reduced by Gata6 overexpression in ES cells

We went on to address whether PRC1/2 binding depends solely on Oct3/4 or on the regulatory system for ES cell self-renewal. Various differentiation cues have been demonstrated to disrupt ES cell self-renewal maintained by the core transcriptional regulatory circuitry. For example, Gata6 has been thought of as a downstream effector of Nanog, and enforced Gata6 expression induces the differentiation program towards extraembryonic endoderm (Chazaud et al., 2006; Fujikura et al., 2002). We therefore examined the effects of the enforced expression of Gata6 on PRC1/2 engagement at Ring1B targets using ES cells expressing a Gata6-GR fusion protein (G6GR) (Shimosato et al., 2007). As previously described, G6GR cells rapidly lose ES-cell-like morphology and show dispersed visceral endoderm-like morphology upon Gata6 activation by the administration of dexamethasone (Dex) (see Fig. S5 in the supplementary material).

We first analyzed the effect of Gata6 activation on the level of PRC1 and PRC2 proteins (Fig. 6A). The level of Ring1B protein was unaffected or only minimally affected during the first 2 days of Dex treatment, but was slightly decreased by day 3. The levels of Phc1, Ezh2, Eed and Suz12 proteins were significantly reduced after Dex treatment, whereas H3K27me3 was unaffected.

Next we used microarray analysis to evaluate the effect of enforced Gata6 expression on gene expression, and compared this profile with those of *Oct3/4*-KO and *Ring1A/B*-dKO ES cells. We found a comparable correlation between Gata6-differentiated and *Ring1A/B*-dKO ES cells (r=0.297), between *Oct3/4*-KO and Gata6-differentiated ES cells (r=0.318), and between *Oct3/4*-KO and *Ring1A/B*-dKO ES cells (r=0.279), not only in terms of total calculable genes but also in genes involved in development,

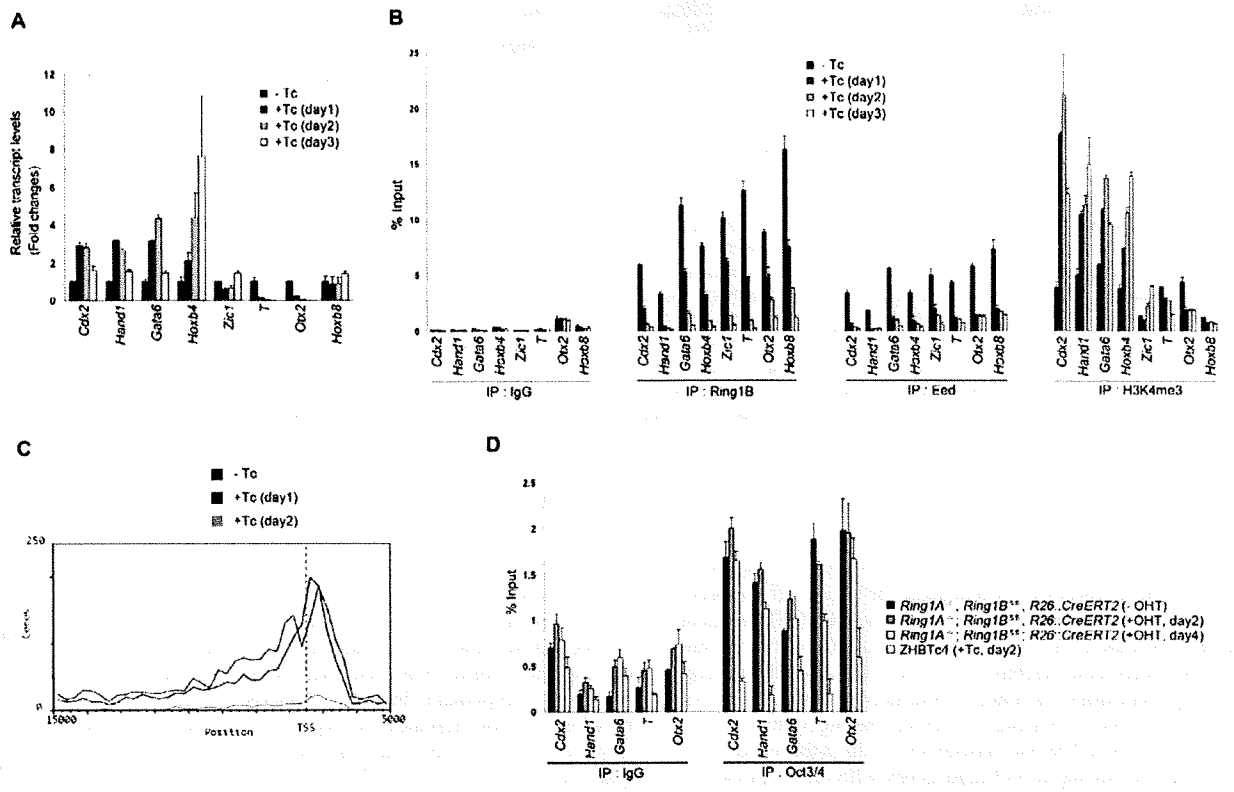

Fig. 4. Oct3/4 is required to engage PRC1 and PRC2 at target gene promoters. (**A**) Changes in expression levels for the selected Ring1B target genes after tetracycline treatment of ZHBTc4 ES cells were determined as described in Fig. 1E. (**B**) ChIP analysis showing binding of Ring1B and Eed and levels of H3K4me3 at the promoter regions of the selected target genes after tetracycline treatment of ZHBTc4 ES cells. The relative amount of immunoprecipitated DNA is depicted as a percentage of input. Error bars represent s.d. determined from at least three independent experiments. (**C**) ChIP-on-chip analysis showing the average Ring1B binding to the promoter regions (from –8 kb to +2 kb relative to the transcription start sites) of the target genes before and after conditional deletion of *Oct3/4*. (**D**) ChIP analysis showing binding of Oct3/4 at the promoter regions of the selected target genes after OHT treatment of *Ring1A*$^{-/-}$;*Ring1B*$^{fl/fl}$;*Rosa26*::*CreERT2* ES cells. The relative amount of immunoprecipitated DNA is depicted as a percentage of input. Error bars represent s.d. determined from at least three independent experiments.

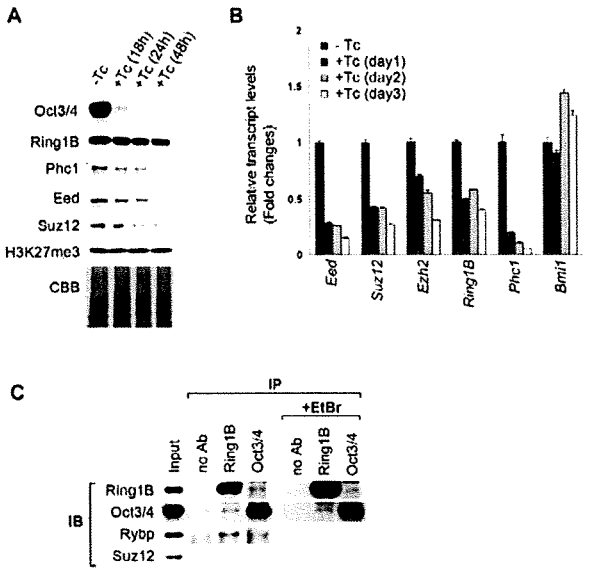

Fig. 5. Possible mechanisms for the reduction in Ring1B binding upon Oct3/4 depletion or differentiation cues. (**A**) Western blot demonstrating changes in the levels of Oct3/4, Ring1B, Phc1, Eed, Suz12 and H3K27me3 after conditional deletion of *Oct3/4* by tetracycline (Tc) treatment of ZHBTc4 ES cells. (**B**) Changes in gene expression levels for *Eed*, *Suz12*, *Ezh2*, *Ring1B*, *Phc1* and *Bmi1* after tetracycline treatment (+Tc) of ZHBTc4 ES cells were determined by real-time PCR, normalized to an *Actb* control and depicted as fold changes relative to the tetracycline-untreated (–Tc) ES cells. Error bars are based on the s.d. derived from triplicate PCR reactions. (**C**) Physical interaction of Ring1B and Oct3/4 in wild-type ES cells demonstrated by reciprocal immunoprecipitation/immunoblot analyses. Antibodies used for immunoprecipitation (IP, top) and immunoblotting (IB, side) are indicated. The association between Ring1B and Oct3/4 proteins remains intact in the presence of ethidium bromide (+EtBr), a DNA-intercalating drug that can disassociate proteins from DNA.

transcription, apoptosis and cell cycle (Fig. 6B). Therefore, a subset of genes induced by enforced Gata6 activation is correlated with those regulated by Oct3/4 and Ring1A/B, suggesting an extension of the functional link to Gata6.

We then investigated whether Gata6 activation affects the levels of Ring1B and Eed at selected Polycomb targets. Of the selected genes, the expression level was increased for *Gata6*, *Cdx2*, *Zic1* and *T*, whereas it was reduced or unchanged for *Hoxb8* and *Hand1* upon Gata6 expression (data not shown). Ring1B binding was significantly reduced irrespective of transcriptional status (Fig. 6C). Phc1 and Eed binding was also reduced (Fig. 6C), consistent with the observed reduction in protein levels (Fig. 6A). These results indicate that Gata6 activation impacts upon gene expression in similar manner to Oct3/4 depletion. Therefore, it is likely that the local engagement of PRC1 depends on the core transcriptional regulatory circuitry rather than solely on Oct3/4 in ES cells.

DISCUSSION

In this study, we first demonstrate that Ring1A/B are required to maintain ES cells in an undifferentiated state by repressing the expression of developmental regulators that direct differentiation of ES cells. This process involves local inhibition of chromatin remodeling via direct binding of PRC1. We further show that Ring1A/B-mediated PcG silencing is hierarchically linked to the core transcriptional regulatory circuitry and that this linkage can be abolished by developmental cues that negatively regulate the core circuitry (Fig. 7). Developmental regulators repressed by this epistatic link, such as *Cdx2* and *Gata6*, are shown to be predisposed for active transcription. Active and reversible repression by this epistatic link is important to potentiate ES cells so that they can respond to developmental cues appropriately and, consequently, it may underpin the maintenance of pluripotency. Therefore, our data show that Ring1A/B are instrumental for the core transcriptional regulatory circuitry to maintain ES cell identity.

The dissociation of PRC1 as a prerequisite for subsequent association of chromatin remodeling components

These and previous studies suggest that PcG proteins are linked to the core transcriptional regulatory circuitry at multiple levels (Fig. 3) (Lee et al., 2006). Oct3/4 is likely to recruit Ring1B to its targets via direct interactions and also to induce the expression of PRC1 components via a transcriptional regulatory mechanism (Fig. 5). Moreover, it is notable that Oct3/4 loss displaces Ring1B from most of its target genes, which are not necessarily functional targets of Oct3/4 (Fig. 4C). This prompts us to postulate an activity that modulates Ring1B recruitment under the regulation of Oct3/4. Indeed, the RING1 and YY1 binding protein, Rybp, potentially fulfils such a linking role between Oct3/4 and Ring1B because Rybp is able to form complexes with both proteins (Fig. 5C) (Wang et al., 2006). Such multiple interactions might enable coordinated displacement of PRC1 and PRC2 from their target genes upon disruption of the core circuitry by differentiation cues. Since forced depletion of *Ring1A/B* leads to spontaneous differentiation of ES cells, dissociation of PRC1 from the targets may be functionally implicated in the differentiation process. We presume that the dissociation of PRC1 and PRC2 is a prerequisite for the subsequent association of other chromatin modifiers such as Trithorax group proteins, which catalyze local hypertrimethylation of H3K4 upon Oct3/4 depletion (Dou et al., 2005; Wysocka et al., 2003). This is supported by our results shown in Fig. 2C, and by previous experiments showing that the SWI-SNF complex is unable to remodel polynucleosomal templates bound by PRC1 in vitro (Shao et al., 1999). Therefore, the global enhancement of chromatin remodeling at developmental genes might be one of the essential events in promoting proper differentiation of ES cells.

Implications from the reversibility of Polycomb binding in the balance of self-renewal versus differentiation

The reversibility of Polycomb binding to the targets regulated by the core transcriptional regulatory circuitry and by differentiation cues might confer self-renewing and differentiation capacities to ES cells. Intriguingly, PcG silencing has been suggested to be involved in the function and maintenance of tissue stem and cancer cells, which are also characterized by both self-renewal and differentiation potency (Lessard and Sauvageau, 2003; Molofsky et al., 2003; Ohta et al., 2002; Park et al., 2003; Villa et al., 2007). For example, *Bmi1* loss promotes differentiation of hematopoietic stem cells (HSCs) and premature senescence of neural stem cells, whereas forced expression of *Bmi1* enhances symmetrical cell division of HSCs (Iwama et al., 2004; Molofsky et al., 2005).

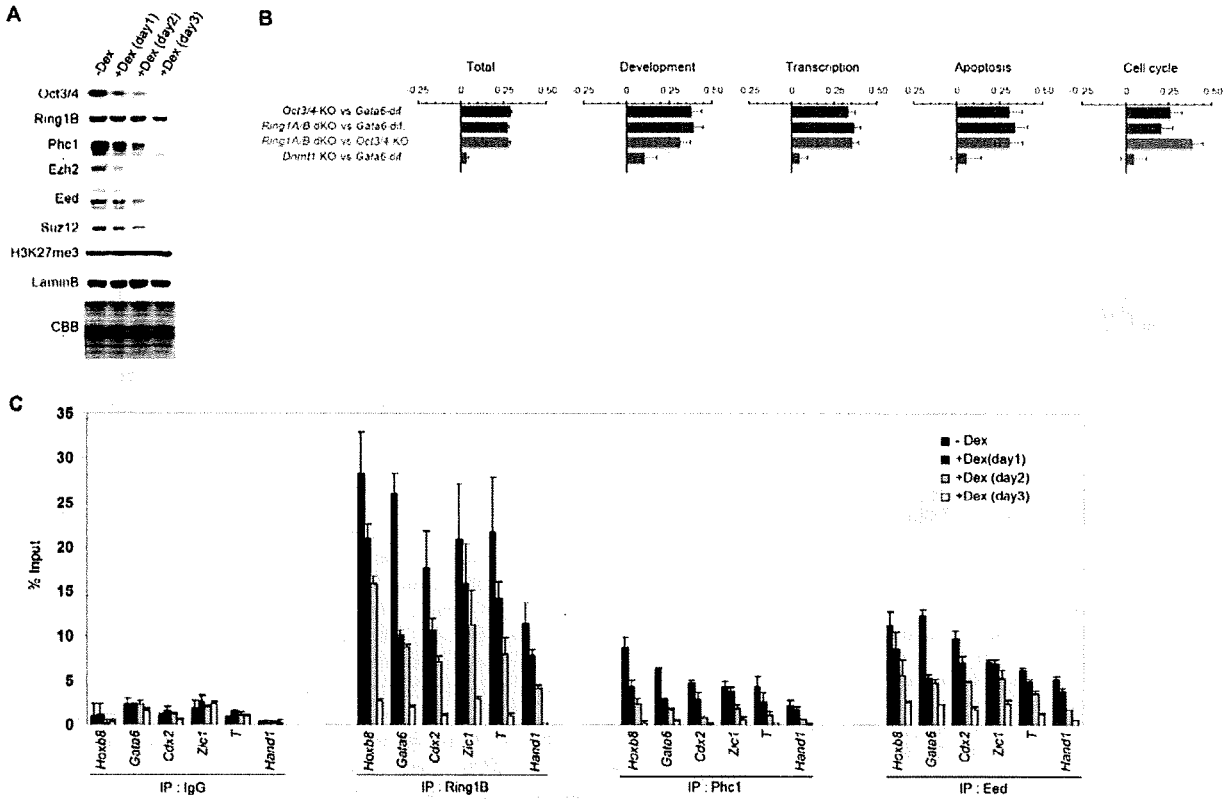

Fig. 6. The engagement of PRC1 and PRC2 is gradually decreased upon Gata6-mediated differentiation of ES cells into primitive endoderm lineages. (**A**) Western blot analysis demonstrating changes in the levels of Oct3/4, Ring1B, Phc1, Ezh2, Eed, Suz12 and H3K27me3 after conditional activation of Gata6 by dexamethasone (Dex) treatment of G6GR ES cells. Lamin B and CBB staining confirmed equal loading. (**B**) Significant overlap of expression profiles in *Ring1A/B*-dKO (day 4), *Oct3/4*-KO (day 1) and Gata6-differentiated (day 2) ES cells. Pearson's correlation of expression changes for probes that belong to specific GO classifications are shown by bars. Functional groupings are indicated above each graph. Error bars represent 95% confidence intervals of correlation coefficients calculated by Z transformation. (**C**) ChIP analysis showing binding of Ring1B, Phc1 and Eed at the promoter regions of the selected target genes after Dex treatment in G6GR ES cells. The relative amount of immunoprecipitated DNA is depicted as a percentage of input. Error bars represent s.d. determined from at least three independent experiments.

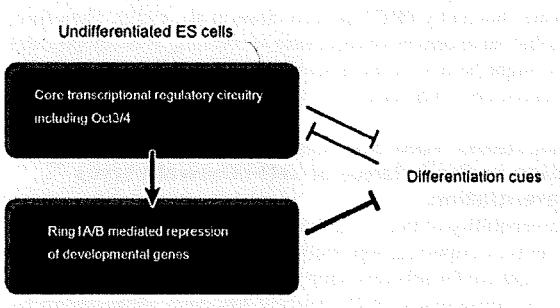

Fig. 7. Schematic representation of the interaction between Ring1A/B and the core transcriptional regulatory circuitry in mouse ES cells. Ring1A/B-mediated PcG silencing functions downstream of the core transcriptional regulatory circuitry including Oct3/4. Developmental cues, such as *Gata6* activation, downregulate the activity of the core transcriptional regulatory circuitry, which accompanies a global decrease in PcG silencing.

Recently, it has been reported that knockdown of *SUZ12* in acute promyelocytic leukemic cells results in myeloid differentiation (Villa et al., 2007). It is thus likely that similar molecular mechanisms identified in ES cells that involve *Ring1A/B* might operate in the maintenance and differentiation of various tissue stem cells and cancer cells. Since *Oct3/4* and *Nanog* are not expressed in most somatic cells, other downstream effectors expressed in common among the stem cells might be more directly involved in the regulation of Polycomb binding. Alternatively, other factors specifically expressed in tissue and/or cancer stem cells might substitute for the action of *Oct3/4* or *Nanog*. Further studies will be needed to clarify these issues.

We thank Hitoshi Niwa for providing ZHBTc4, G6GR and ZHTc6 cells. This work was supported in part by a grant from the Genome Network Project (to H.K.) and a grant-in-aid for Scientific Research on Priority Areas (17045038, to M.E.) from the Ministry of Education, Culture, Sports, Science and Technology, Japan.

Supplementary material

Supplementary material for this article is available at http://dev.biologists.org/cgi/content/full/135/8/1513/DC1

References

Androutsellis-Theotokis, A., Leker, R. R., Soldner, F., Hoeppner, D. J., Ravin, R., Poser, S. W., Rueger, M. A., Bae, S. K., Kittappa, R. and McKay, R. D. (2006). Notch signalling regulates stem cell numbers in vitro and in vivo. *Nature* **442**, 823-826.

Atsuta, T., Fujimura, S., Moriya, H., Vidal, M., Akasaka, T. and Koseki, H. (2001). Production of monoclonal antibodies against mammalian Ring1B proteins. *Hybridoma* **20**, 43-46.

Auernhammer, C. J. and Melmed, S. (2000). Leukemia-inhibitory factor-neuroimmune modulator of endocrine function. *Endocr. Rev.* **21**, 313-345.

Avilion, A. A., Nicolis, S. K., Pevny, L. H., Perez, L., Vivian, N. and Lovell-Badge, R. (2003). Multipotent cell lineages in early mouse development depend on SOX2 function. *Genes Dev.* **17**, 126-140.

Azuara, V., Perry, P., Sauer, S., Spivakov, M., Jorgensen, H. F., John, R. M., Gouti, M., Casanova, M., Warnes, G., Merkenschlager, M. et al. (2006). Chromatin signatures of pluripotent cell lines. *Nat. Cell Biol.* **8**, 532-538.

Bernstein, B. E., Mikkelsen, T. S., Xie, X., Kamal, M., Huebert, D. J., Cuff, J., Fry, B., Meissner, A., Wernig, M., Plath, K. et al. (2006). A bivalent chromatin structure marks key developmental genes in embryonic stem cells. *Cell* **125**, 315-326.

Bolstad, B. M., Irizarry, R. A., Astrand, M. and Speed, T. P. (2003). A comparison of normalization methods for high density oligonucleotide array data based on variance and bias. *Bioinformatics* **19**, 185-193.

Boyer, L. A., Lee, T. I., Cole, M. F., Johnstone, S. E., Levine, S. S., Zucker, J. P., Guenther, M. G., Kumar, R. M., Murray, H. L., Jenner, R. G. et al. (2005). Core transcriptional regulatory circuitry in human embryonic stem cells. *Cell* **122**, 947-956.

Boyer, L. A., Plath, K., Zeitlinger, J., Brambrink, T., Medeiros, L. A., Lee, T. I., Levine, S. S., Wernig, M., Tajonar, A., Ray, M. K. et al. (2006). Polycomb complexes repress developmental regulators in murine embryonic stem cells. *Nature* **441**, 349-353.

Buchwald, G., van der Stoop, P., Weichenrieder, O., Perrakis, A., van Lohuizen, M. and Sixma, T. K. (2006). Structure and E3-ligase activity of the Ring-Ring complex of polycomb proteins Bmi1 and Ring1b. *EMBO J.* **25**, 2465-2474.

Burdon, T., Smith, A. and Savatier, P. (2002). Signalling, cell cycle and pluripotency in embryonic stem cells. *Trends Cell Biol.* **12**, 432-438.

Cales, C., Roman-Trufero, M., Pavon, L., Serrano, I., Melgar, T., Endoh, M., Perez, C., Koseki, H. and Vidal, M. (2008). Inactivation of the polycomb group protein Ring1B unveils an antiproliferative role in hematopoietic cell expansion and cooperation with tumorigenesis associated with Ink4a deletion. *Mol. Cell. Biol.* **28**, 1018-1028.

Cao, R., Wang, L., Wang, H., Xia, L., Erdjument-Bromage, H., Tempst, P., Jones, R. S. and Zhang, Y. (2002). Role of histone H3 lysine 27 methylation in Polycomb-group silencing. *Science* **298**, 1039-1043.

Catena, R., Tiveron, C., Ronchi, A., Porta, S., Ferri, A., Tatangelo, L., Cavallaro, M., Favaro, R., Ottolenghi, S., Reinbold, R. et al. (2004). Conserved POU binding DNA sites in the Sox2 upstream enhancer regulate gene expression in embryonic and neural stem cells. *J. Biol. Chem.* **279**, 41846-41857.

Chambers, I., Colby, D., Robertson, M., Nichols, J., Lee, S., Tweedie, S. and Smith, A. (2003). Functional expression cloning of Nanog, a pluripotency sustaining factor in embryonic stem cells. *Cell* **113**, 643-655.

Chazaud, C., Yamanaka, Y., Pawson, T. and Rossant, J. (2006). Early lineage segregation between epiblast and primitive endoderm in mouse blastocysts through the Grb2-MAPK pathway. *Dev. Cell* **10**, 615-624.

Czermin, B., Melfi, R., McCabe, D., Seitz, V., Imhof, A. and Pirrotta, V. (2002). Drosophila enhancer of Zeste/ESC complexes have a histone H3 methyltransferase activity that marks chromosomal Polycomb sites. *Cell* **111**, 185-196.

Dou, Y., Milne, T. A., Tackett, A. J., Smith, E. R., Fukuda, A., Wysocka, J., Allis, C. D., Chait, B. T., Hess, J. L. and Roeder, R. G. (2005). Physical association and coordinate function of the H3 K4 methyltransferase MLL1 and the H4 K16 acetyltransferase MOF. *Cell* **121**, 873-885.

de Napoles, M., Mermoud, J. E., Wakao, R., Tang, Y. A., Endoh, M., Appanah, R., Nesterova, T. B., Silva, J., Otte, A. P., Vidal, M. et al. (2004). Polycomb group proteins Ring1A/B link ubiquitylation of histone H2A to heritable gene silencing and X inactivation. *Dev. Cell* **7**, 663-676.

del Mar Lorente, M., Marcos-Gutierrez, C., Perez, C., Schoorlemmer, J., Ramirez, A., Magin, T. and Vidal, M. (2000). Loss- and gain-of-function mutations show a polycomb group function for Ring1A in mice. *Development* **127**, 5093-5100.

Evans, M. J. and Kaufman, M. H. (1981). Establishment in culture of pluripotential cells from mouse embryos. *Nature* **292**, 154-156.

Fischle, W., Wang, Y., Jacobs, S. A., Kim, Y., Allis, C. D. and Khorasanizadeh, S. (2003). Molecular basis for the discrimination of repressive methyl-lysine marks in histone H3 by Polycomb and HP1 chromodomains. *Genes Dev.* **17**, 1870-1881.

Fujikura, J., Yamato, E., Yonemura, S., Hosoda, K., Masui, S., Nakao, K., Miyazaki, J.-i., and Niwa, H. (2002). Differentiation of embryonic stem cells is induced by GATA factors. *Genes Dev.* **16**, 784-789.

Fujimura, Y., Isono, K., Vidal, M., Endoh, M., Kajita, H., Mizutani-Koseki, Y., Takihara, Y., van Lohuizen, M., Otte, A., Jenuwein, T. et al. (2006). Distinct roles of Polycomb group gene products in transcriptionally repressed and active domains of Hoxb8. *Development* **133**, 2371-2381.

Garcia, E., Marcos-Gutierrez, C., del Mar Lorente, M., Moreno, J. C. and Vidal, M. (1999). RYBP, a new repressor protein that interacts with components of the mammalian Polycomb complex, and with the transcription factor YY1. *EMBO J.* **18**, 3404-3418.

Hamer, K. M., Sewalt, R. G., den Blaauwen, J. L., Hendrix, T., Satijn, D. P. and Otte, A. P. (2002). A panel of monoclonal antibodies against human polycomb group proteins. *Hybrid Hybridomics* **21**, 245-252.

Heinrich, P. C., Behrmann, I., Haan, S., Hermanns, H. M., Muller-Newen, G. and Schaper, F. (2003). Principles of interleukin (IL)-6-type cytokine signalling and its regulation. *Biochem. J.* **374**, 1-20.

Isono, K., Fujimura, Y.-i, Shinga, J., Yamaki, M., O-Wang, J., Takihara, Y., Murahashi, Y., Takada, Y., Mizutani-Koseki, Y. and Koseki, H. (2005a). Mammalian polyhomeotic homologues Phc2 and Phc1 act in synergy to mediate polycomb repression of Hox genes. *Mol. Cell. Biol.* **25**, 6694-6706.

Isono, K., Mizutani-Koseki, Y., Komori, T., Schmidt-Zachmann, M. S. and Koseki, H. (2005b). Mammalian polycomb-mediated repression of Hox genes requires the essential spliceosomal protein Sf3b1. *Genes Dev.* **19**, 536-541.

Iwama, A., Oguro, H., Negishi, M., Kato, Y., Morita, Y., Tsukui, H., Ema, H., Kamijo, T., Katoh-Fukui, Y., Koseki, H. et al. (2004). Enhanced self-renewal of hematopoietic stem cells mediated by the polycomb gene product Bmi-1. *Immunity* **21**, 843-851.

Kuroda, T., Tada, M., Kubota, H., Kimura, H., Hatano, S. Y., Suemori, H., Nakatsuji, N. and Tada, T. (2005). Octamer and Sox elements are required for transcriptional cis regulation of Nanog gene expression. *Mol. Cell. Biol.* **25**, 2475-2485.

Kuzmichev, A., Nishioka, K., Erdjument-Bromage, H., Tempst, P. and Reinberg, D. (2002). Histone methyltransferase activity associated with a human multiprotein complex containing the Enhancer of Zeste protein. *Genes Dev.* **16**, 2893-2905.

Lai, J. S. and Herr, W. (1992). Ethidium bromide provides a simple tool for identifying genuine DNA-independent protein associations. *Proc. Natl. Acad. Sci. USA* **89**, 6958-6962.

Lee, T. I., Jenner, R. G., Boyer, L. A., Guenther, M. G., Levine, S. S., Kumar, R. M., Chevalier, B., Johnstone, S. E., Cole, M. F., Isono, K. et al. (2006). Control of developmental regulators by Polycomb in human embryonic stem cells. *Cell* **125**, 301-313.

Leeb, M. and Wutz, A. (2007). Ring1B is crucial for the regulation of developmental control genes and PRC1 proteins but not X inactivation in embryonic cells. *J. Cell Biol.* **178**, 219-229.

Lei, H., Oh, S. P., Okano, M., Juttermann, R., Goss, K. A., Jaenisch, R. and Li, E. (1996). De novo DNA cytosine methyltransferase activities in mouse embryonic stem cells. *Development* **122**, 3195-3205.

Lessard, J. and Sauvageau, G. (2003). Bmi-1 determines the proliferative capacity of normal and leukaemic stem cells. *Nature* **423**, 255-260.

Loh, Y. H., Wu, Q., Chew, J. L., Vega, V. B., Zhang, W., Chen, X., Bourque, G., George, J., Leong, B., Liu, J. et al. (2006). The Oct4 and Nanog transcription network regulates pluripotency in mouse embryonic stem cells. *Nat. Genet.* **38**, 431-440.

Martin, G. R. (1981). Isolation of a pluripotent cell line from early mouse embryos cultured in medium conditioned by teratocarcinoma stem cells. *Proc. Natl. Acad. Sci. USA* **78**, 7634-7638.

Matoba, R., Niwa, H., Masui, S., Ohtsuka, S., Carter, M. G., Sharov, A. A. and Ko, M. S. (2006). Dissecting oct3/4-regulated gene networks in embryonic stem cells by expression profiling. *PLoS ONE* **1**, e26.

Min, J., Zhang, Y. and Xu, R. M. (2003). Structural basis for specific binding of Polycomb chromodomain to histone H3 methylated at Lys 27. *Genes Dev.* **17**, 1823-1828.

Mitsui, K., Tokuzawa, Y., Itoh, H., Segawa, K., Murakami, M., Takahashi, K., Maruyama, M., Maeda, M. and Yamanaka, S. (2003). The homeoprotein Nanog is required for maintenance of pluripotency in mouse epiblast and ES cells. *Cell* **113**, 631-642.

Miyagishima, H., Isono, K., Fujimura, Y., Iyo, M., Takihara, Y., Masumoto, H., Vidal, M. and Koseki, H. (2003). Dissociation of mammalian Polycomb-group proteins, Ring1B and Rae28/Ph1, from the chromatin correlates with configuration changes of the chromatin in mitotic and meiotic prophase. *Histochem. Cell Biol.* **120**, 111-119.

Molofsky, A. V., Pardal, R., Iwashita, T., Park, I. K., Clarke, M. F. and Morrison, S. J. (2003). Bmi-1 dependence distinguishes neural stem cell self-renewal from progenitor proliferation. *Nature* **425**, 962-967.

Molofsky, A. V., He, S., Bydon, M., Morrison, S. J. and Pardal, R. (2005). Bmi-1 promotes neural stem cell self-renewal and neural development but not mouse growth and survival by repressing the p16Ink4a and p19Arf senescence pathways. *Genes Dev.* **19**, 1432-1437.

Muller, J., Hart, C. M., Francis, N. J., Vargas, M. L., Sengupta, A., Wild, B., Miller, E. L., O'Connor, M. B., Kingston, R. E. and Simon, J. A. (2002).